which the naphthyridine dimer was covalently bound through 3, 2, and 1 PEO units, respectively. The buffer used for the analysis was 10 mM of HEPES (pH = 7.4) containing 150 mM of NaCl. The measurements were carried out at 25 °C. Because the degree of immobilization of the ligand on the surface was different for **Sensors 1**, **3**, and **4**, the SPR intensity was normalized, and was quoted in units of mass of DNA bound to a unit per immobilized ligands (pg of DNA per pmol of an immobilized ligand) (Fig. 2). A prototype of the sensor where **2** was immobilized showed a signal intensity of 94 pg·pmol^{-1} after a period of 180 s after the injection of **CGG/GCC**. As can be seen from Figure 2, the SPR intensity increased to 1.5×10^2, 4.9×10^2, and 1.2×10^3 pg·pmol^{-1} as increasing the number of PEO units incorporated in the linker from one to three. The signal obtained for **Sensor 1** is about 13-fold stronger in intensity than that obtained for **2**-immobilized sensor. Further incorporation of the PEO unit in the linker did not produce remarkable signal enhancement.

Having found that the incorporation of three PEO units significantly increased the SPR intensity, we then determined the detection limit of the G–G mismatch duplex by using **Sensor 2**. A distinct SPR signal was observed for CGG/GGC at a concentration of 1 nM, whereas duplexes containing a G–A mismatch (XYZ/X′Y′Z′ = CGG/GAC), a G–T mismatch (XYZ/X′Y′Z′ = CGG/GTC), and a G–C match (XYZ/X′Y′Z′ = CGG/GCC) base pair did not show any significant signal (Fig. 3). Further lowering of the concentration of CGG/GGC resulted in a loss of signal. By using a refined linker with three PEO units for the immobilization of the naphthyridine dimer and the Biacore 2000 instrument, a concentration of 1 nM for the 27-mer duplex was found to be the lower limit for the detection of the G–G mismatch. Because the SPR intensity increased with increasing molecular weight of the analyte, the detection limit of longer duplexes containing the G–G mismatch would be below 1 nM.

The effect of the sequence flanking to the G–G mismatch on the SPR detection by the **1**-immobilized surface was investigated by analyzing 10 G–G mismatches by **Sensor 1**. The sensorgrams were obtained by applying 1 μM of XYZ/X′Y′Z′ to Sensor 1. The SPR signals for all the G–G mismatches were clearly detected and

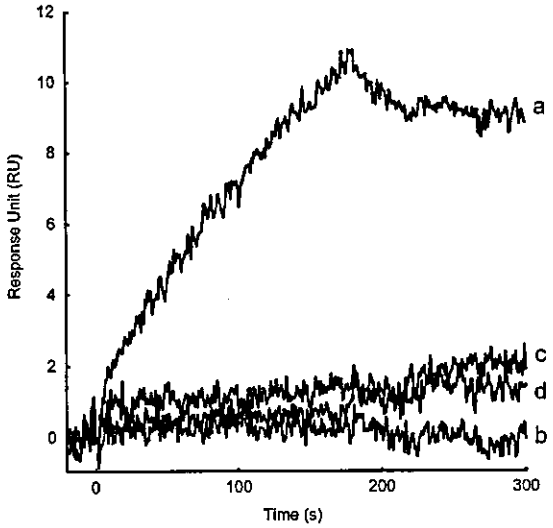

Figure 3. Detection of mismatched DNAs at a concentration of 1 nM by **Sensor 2**. Key: (a) CGG/GGC, (b) CGG/GAC, (c) CGG/GTC, and (d) CGG/GCC.

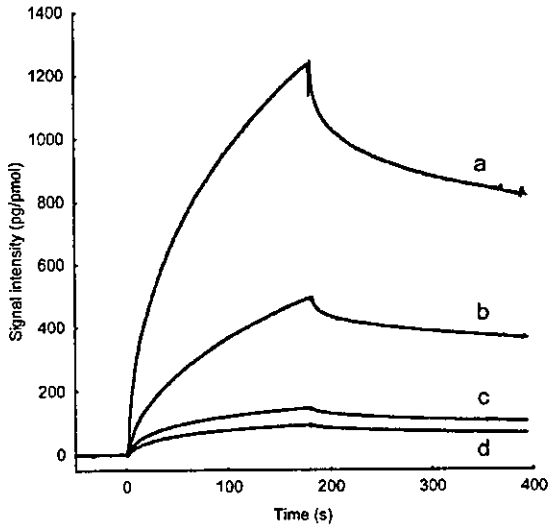

Figure 2. Binding of 27-mer duplex 5′-d(GTT ACA GAA TCT XYZ AAG CCT AAT ACG)-3′/3′-d(CAA TGT CTT AGA X′Y′Z′ TTC GGA TTA TGC)-5′ (1.0 μM) containing the G–G mismatch (XYZ/X′Y′Z′ = CGG/GGC) to the naphthyridine dimer-immobilized sensors (**Sensors 1**, **3**, and **4**) possessing a different length of PEO unit. Key: (a) **Sensor 1**, (b) **Sensor 3**, (c) **Sensor 4**, and (d) **2**-immobilized sensor. The signal intensity represents an amount of DNA (pg) bound to a unit amount (pmol) of each immobilized ligand on the surface.

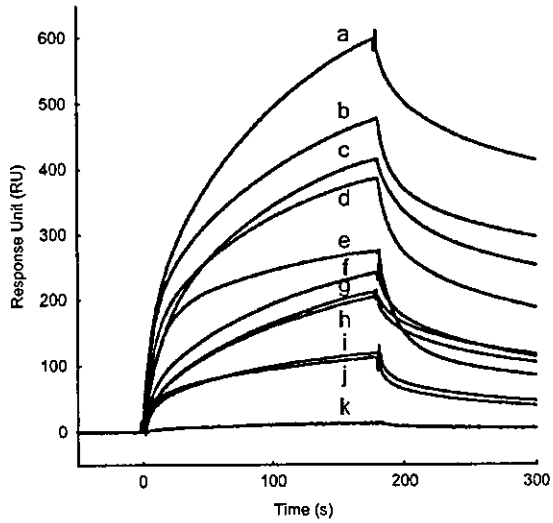

Figure 4. Sensorgrams obtained for the binding of XYZ/X′Y′Z′ to **Sensor 1** at a concentration of 1 μM duplex. Binding was measured for 180 s and dissociation for 120 s. Key: (a) GGC/CGG, (b) CGG/GGC, (c) CGC/GGG, (d) TGG/AGC, (e) TGA/AGT, (f) AGG/TGC, (g) TGC/AGG, (h) AGC/TGG, (i) AGA/TGT, (j) AGT/TGA, (k) CGG/GAC (GA mismatch).

sequence dependent on the flanking base pairs (Fig. 4). The strongest SPR signal was observed for the GGC/CGG, whereas the weakest signal was observed for AGT/TGA. The difference in SPR intensity between these two G–G mismatches is about 6 folds. The G–G mismatches flanking G–C base pairs binds to the **1**-immobilized surface stronger than those flanking A–T base pairs. These observations are in good agreement with the results obtained by DNase I foot print titration and UV-melting studies of duplexes containing the G–G mismatch in the presence of **1**.[15] In contrast, the SPR signal observed for the G–A mismatch was quite weak as compared to those of the G–G mismatch. These results showed that **Sensor 1** is capable of detecting the G–G mismatch in duplex DNA irrespective of the sequence flanking to the mismatch.

Unlike most SPR studies using the surfaces where macromolecules were immobilized, the drug-immobilized surface was extremely sensitive to the way of drug immobilization due to a small molecular size relative to the surface and its hydrophobic character. The studies described here reveal that incorporation of three PEO linker units between naphthyridine dimer and the dextran surface is especially effective in increasing the SPR sensitivity without losing the mismatch specificity.

Acknowledgements

This work was supported by Grant-in-Aid for Scientific Research on Priority Areas (C) 'Medical Genome Science' from the Ministry of Education, Culture, Sports, Science and Technology of Japan.

References and notes

1. Syvänen, A.-C. *Nat. Rev. Gen.* **2001**, *2*, 930.
2. Kwok, P. Y. *Annu. Rev. Genom. Hum. G* **2001**, *2*, 235.
3. Schafer, A. J.; Hawkins, J. R. *Nat. Biotechnol.* **1998**, *16*, 33.
4. Nakatani, K.; Sando, S.; Saito, I. *Nat. Biotechnol.* **2001**, *19*, 51.
5. Nakatani, K.; Sando, S.; Kumasawa, H.; Kikuchi, J.; Saito, I. *J. Am. Chem. Soc.* **2001**, *123*, 12650.
6. Nakatani, K.; Sando, S.; Saito, I. *Bioorg. Med. Chem.* **2001**, *9*, 2381.
7. Smith, E. A.; Kyo, M.; Kumasawa, H.; Nakatani, K.; Saito, I.; Corn, R. M. *J. Am. Chem. Soc.* **2002**, *124*, 6810.
8. Nakatani, K.; Hagihara, S.; Sando, S.; Sakamoto, S.; Yamaguchi, K.; Maesawa, C.; Saito, I. *J. Am. Chem. Soc.* **2003**, *125*, 662.
9. Kobori, A.; Horie, S.; Suda, H.; Saito, I.; Nakatani, K. *J. Am. Chem. Soc.* **2004**, *126*, 557.
10. Hagihara, S.; Kumasawa, H.; Goto, Y.; Hayashi, G.; Kobori, A.; Saito, I.; Nakatani, K. *Nucleic Acids Res.* **2004**, *32*, 278.
11. Jackson, B. A.; Barton, J. K. *J. Am. Chem. Soc.* **1997**, *119*, 12986.
12. Jackson, B. A.; Alekseyev, V. Y.; Barton, J. K. *Biochemistry* **1999**, *38*, 4655.
13. Lacy, E. R.; Cox, K. K.; Wilson, W. D.; Lee, M. *Nucleic Acids Res.* **2002**, *30*, 1834.
14. Landers, J. P. *Anal. Chem.* **2003**, *75*, 2919.
15. Nataraj, A. J.; Olivos-Glander, I.; Kusukawa, N. *Electrophoresis* **1999**, *20*, 1177.
16. Pharmacia-Biosensor. 1990 *Biacore User's Manual.* Piscatway, NJ.
17. Jeong, S. W.; O'Brien, D. F. *J. Org. Chem.* **2001**, *66*, 4799.
18. Boumrah, D.; Campbell, M. M.; Fenner, S.; Kinsman, R. G. *Tetrahedron* **1997**, *53*, 6977.
19. Lõfås, S.; Johnson, B. *J. Chem. Soc., Chem. Commun.* **1990**, *21*, 1526.

Solvent Effects on the Suppression of Oxidative Decomposition of Guanines by Phenyl Group Attachment in Deoxyribonucleic Acid (DNA)

Satoshi Yokojima,[†,‡] Wataru Yanoi,[‡] Norifumi Yoshiki,[‡] Noriyuki Kurita,[§] Shigenori Tanaka,[⊥] Kazuhiko Nakatani,[†,∥] and Akira Okada*[,‡]

Japan Science and Technology Corporation (JST), 4-1-8 Honcho, Kawaguchi 332-0012, Japan, Institute of Materials Science, University of Tsukuba, 1-1-1, Ten-nodai, Tsukuba 305-8573, Japan, Department of Knowledge-Based, Information Engineering, Toyohashi University of Technology, Tempaku-cho, Toyohashi 441-8580, Japan, Advanced Materials and Devices Laboratory, Toshiba R&D Center, Kawasaki 212-8582, Japan, Department of Synthetic Chemistry and Biological Chemistry, Faculty of Engineering, Kyoto University, PRESTO, JST, Kyoto 606-8501, Japan

Received: December 12, 2003; In Final Form: February 13, 2004

A recent experimental report on the suppression of the oxidative decomposition of guanines in deoxyribonucleic acid (DNA) double helices due to the attachment of a phenyl group to a guanine [Nakatani, K.; Dohno, C.; Saito, I. *J. Am. Chem. Soc.* **2002**, *124*, 6802] is examined by semiempirical Hartree−Fock (HF) molecular orbital (MO) calculations and ab initio HF MO calculations with the STO-3G basis set. Because of this attachment, the energy level of MO localized on the guanine shifts to lower energy in a vacuum, whereas it shifts to higher energy in water. This is mainly because the energy reduction of MO levels by the water solvent becomes smaller when the solvent molecules are excluded by the phenyl group. Consequently, a hole trap is enhanced at the phenylated guanine base in water. The observed suppression of the oxidative decomposition of guanines around the phenylated guanine is thus explained by considering the solvent effects. In addition, we have observed that energy shifts due to a benzyl group or a *tert*-butyl group are similar to those due to the phenyl group in our calculation.

1. Introduction

Deoxyribonucleic acid (DNA) is one of the candidates for next-generation electronic devices,[1] because of the full controllability of its sequence, the self-assembling feature, and the conducting properties. Especially, the conducting properties of DNA have attracted much attention in recent years and numerous experimental studies have been reported.[2−6] However, there are some obstacles to use DNA as a molecular device. One of the obstacles is the oxidative decomposition; i.e., DNA can easily be oxidized and subsequently decomposed at the guanine bases.[2,6−13] Recently, it has been reported that the oxidative decomposition is dramatically suppressed by attaching a phenyl group to a guanine in a double-stranded oligodeoxynucleotide (ODN).[14] To suppress the oxidative decomposition further, it is important to understand the role of N^2-phenyldeoxyguanosine in DNA.

Stimulated by the experimental studies, theoretical analysis of the conducting properties of DNA has been performed by many groups.[15−33] For those analyses, the electronic structure calculation gives a lot of information that is related to the energetics and kinetics.[28−33] For the study of the electronic structure of DNA, it is important to include the solvent effect. However, most of the earlier calculations of the electronic structure of DNA are conducted in a vacuum, mainly because the calculation including the solvent effect for this large molecule is computationally demanding. As small fragments of DNA, the solvent effect on the ionization potential of nucleotides and a phosphorylated dinucleotide with counterions has been studied intensively.[29,30] More recently, much-larger-sized DNA systems have been studied including the solvent effect.[31−33] These studies further confirm the importance of the solvent effect on the electronic properties of DNA.

In this paper, we analyze the energetics of the phenyl group attachment to a guanine. One of the interesting results found in ref 14 is that the oxidative decomposition is suppressed not only at the phenylated guanine but also at the guanines around the phenylated one. If the role of the phenyl group is only to suppress the deprotonation of the phenylated guanine radical cation,[8,34−36] a hole at the phenylated guanine has a greater chance to be transferred to the neighboring guanine bases and their oxidative decomposition will increase, which contradicts the experimental observation.[14] To explain the experimental results, we must examine energetics of this system. Here, we perform semiempirical Hartree−Fock (HF) molecular orbital (MO) calculations and ab initio HF MO calculations with the STO-3G basis set and find that the energy level of MO localized on the guanine shifts to lower energy in a vacuum, whereas it shifts to higher energy in water because of the attachment of a phenyl group to a guanine. This is mainly because the energy reduction of MO levels by the water solvent becomes smaller when the solvent molecules are excluded by the phenyl group. Consequently, a hole trap is enhanced at the phenylated guanine base in water and guanines around the phenylated one have fewer chances to trap a hole. The observed suppression of the

* Author to whom correspondence should be addressed. E-mail address: aokada@ims.tsukuba.ac.jp.
† JST.
‡ University of Tsukuba.
§ Toyohashi University of Technology.
⊥ Toshiba R&D Center.
∥ Kyoto University, PRESTO.

10.1021/jp037845s CCC: $27.50
Published on Web 05/04/2004

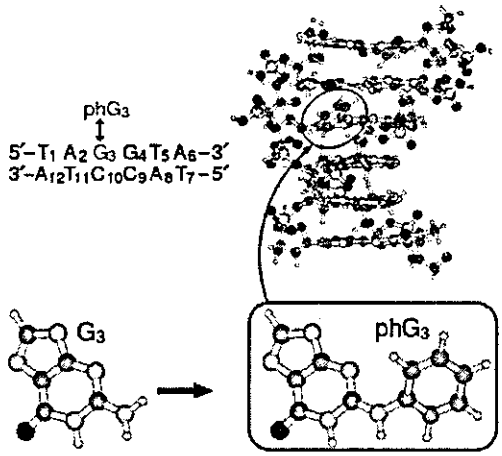

Figure 1. Structure of ODN ^{Ph}GG. The numbers of atoms of ODN GG and ODN ^{Ph}GG are 390 and 400, respectively. The approximate dimension of ODN GG is given as follows: (1) the distances between the two P atoms located between the stacked Watson−Crick base pairs are 17.76 and 18.21 Å for the 4th and 55th fiber model structures, respectively; (2) the distances between the N1 site of the adenine at each end of ODN GG are 16.85 and 16.98 Å for the 4th and 55th fiber model structures, respectively.

oxidative decomposition of guanines around the phenylated guanine[14] is thus explained by the solvent effects on the energetics of DNA.

The paper is organized as follows. In Section 2, we explain the methods in our calculations, such as the preparation of the DNA structure, semiempirical and ab initio HF MO calculations, and solvent models. In Section 3, the energy shift due to the phenyl group attachment to a guanine in a double-stranded ODN is shown as a main result. To assess the validity of our calculations, we also show the results with other models, i.e., other semiempirical HF MO calculations, and ab initio HF MO calculations with the STO-3G basis set. We then explain the relation between the energy shift and the observed suppression of the oxidative decomposition of guanines around the phenylated guanine.[14] To clarify the origin of the energy shift, the result is compared to the calculation of DNA with a H_2 cluster (10 H_2 molecules) in place of the phenyl group, where the H_2 cluster mimics the solvent-accessible surface of the phenyl group. The solvent effect is further examined for DNA molecules with other functional groups attached: a benzyl-group-attached DNA and a *tert*-butyl-group-attached DNA. Finally, conclusions are given in Section 4.

2. Methods

The sequence 5′-TAGGTA-3′ and its phenylated counterpart 5′-TA^{Ph}GGTA-3′ appear as a part of the oligomers investigated in ref 14. We denote the former as ODN GG and latter as ODN ^{Ph}GG (see Figure 1). The B-DNA structure of ODN GG with backbones is constructed by the 3DNA v1.5 program.[37] To ensure that our conclusion is not dependent on the structure, we have chosen two typical B-DNA structures in the calculation, i.e., the 4th[38] and 55th[39] fiber models (see Tables S1 and S10 in the Supporting Information). These fiber models are determined by X-ray diffraction analysis. Therefore, only the positions of the heavy atoms are identified. H atoms are attached, and their positions are optimized using Austin Model 1 (AM1)[40] in the MOPAC2002 v1.0 program.[41] (We do not use the linear scaling calculation program MOZYME that is implemented in MOPAC2002.) The geometry optimization of the H atoms in the water solvent is performed by AM1 with the conductor-like screening model (COSMO).[42,43] The structure of ODN ^{Ph}GG is obtained by attaching the phenyl group to ODN GG and optimizing the geometry of the phenyl group by AM1 (AM1/COSMO) in a vacuum (water). Both the 4th and 55th fiber models have similar global structural parameters; i.e., the helical twists are 36° for both fiber models, and the rises are 3.38 and 3.39 Å for the 4th and 55th fiber models, respectively. The structural differences between these two fiber models are mainly found in the sugar−phosphate backbone parameters. The structures used in the calculations are given in Tables S1−S18 in the Supporting Information.

TABLE 1: Differences in Vertical Ionization Potentials (IPs) between Guanine and other DNA Bases, and Differences in Oxidation Potentials (OPs) between Deoxyguanosine and Other Nucleosides[a]

	IP (eV)			OP (V)		
				AM1		
	AM1	experiment[b]		optimized vdW radii[c]	default vdW radii[d]	experiment
A	0.09	0.20	dA	0.23	0.16	0.49[e]
C	0.70	0.70	dC	0.76	0.63	0.65[e]
T	0.93	0.90	dT	0.73	0.58	0.62[e]
			d^{ph}G	−0.01	−0.17	0.03[f]

[a] The geometries are optimized by AM1. [b] Data from ref 44. [c] Data from ref 43. [d] Data from ref 41. [e] Data from ref 45. [f] Data from ref 14.

The electronic structure calculation is performed by the AM1 Hamiltonian[40] implemented in a semiempirical MO program MOPAC2002.[41] The solvent effect is taken into account by a continuum solvent model, i.e., COSMO.[42,43] We use the Koopmans theorem to examine the energy shifts of MO energy levels near the highest occupied molecular orbital (HOMO) of ODNs. The use of this method is justified in the following.

(1) As for the validity of the Koopmans theorem with AM1 and COSMO, we calculate the relative ionization potentials (IPs) for bases in a vacuum and the relative oxidation potentials (OPs) for nucleosides in water and compare them to experiments. The root-mean-square (RMS) deviations between computational and experimental results[14,44,45] are 0.07 eV and 0.15 V (Table 1) for IPs and OPs, respectively.

(2) The aforementioned energy shifts obtained by the Koopmans theorem do not include the difference of the reorganization energies between the guanine and phenylated guanine. However, this difference, as evaluated from the experimental results,[46] is less than ~0.13 eV (see Appendix for details). These values are smaller than the energy change that is due to the attachment of the phenyl group obtained by the Koopmans theorem and, therefore, do not change our conclusion.

Our conclusions obtained uisng the AM1/COSMO calculations are further confirmed by different models, i.e., (i) the MNDO−Parametric Method 3 (PM3) Hamiltonian[47] with the COSMO in MOPAC2002 and (ii) the generalized Born (GB) model[48] implemented in ABINIT/GB, which is an ab initio MO/GB program package.[49] The PM3 calculation is performed in a manner similar to that for the AM1 calculation, except that the geometries of H atoms and the phenyl group are optimized by PM3. The ABINIT/GB calculations are performed with the STO-3G basis set. We use the 4th fiber model structure, and the geometries of H atoms and the phenyl group are optimized by AM1.

The parameters used for the COSMO calculation are given as follows. The dielectric constant of water is taken as $\epsilon = 78.4$. Because the van der Waals (vdW) parameters of COSMO

implemented in MOPAC2002 are not optimized, we use the optimized vdW parameters of COSMO for the density functional formalism (DFT) calculation.[43] Those optimized vdW parameters are expected to produce better results than the default vdW parameters of COSMO[50] (see the Supporting Information). In fact, the RMS deviation between the experimental relative OPs[14,45] and the computational OPs with the default vdW parameters of COSMO in MOPAC2002[41] is 0.19 V, which is larger than that with the optimized vdW parameters (i.e., 0.15 V; see Table 1). Among the optimized vdW radii, the vdW radius for the P atom is not reported in ref 43. Instead, we use a suggested value of 2.106 Å as the vdW radius for the P atom.[50] To assess whether the results in the following are unaffected by the vdW radius of the P atom, we have also performed the calculations for different vdW radii of the P atom (i.e., 1.906 and 2.306 Å) and found that the results change little.

We report the results of the neutral DNA in water and in a vacuum in the following, because the positions of the counterions have been observed to have little effect on the energy differences between the HOMO and other occupied MOs near the HOMO in the calculations including the water solvent as follows. The calculations in the water solvent have been performed by considering ODN GG (ODN ^{Ph}GG) in both neutral and ionic states. The calculations of ODN GG (ODN ^{Ph}GG) in ionic states have been performed by eliminating 10 H atoms at the phosphate backbones and assigning the total charge of −10. Our ionic state calculation corresponds to the case where the counterions are far away from the DNA molecule, compared to the solvent layers that are surrounding the DNA molecule. The actual DNA molecule in an ionic state should be between the neutral and our ionic state calculations. Our ionic state calculation only gives mere energy shifts of 0.26−0.32 eV (see Table S19 in the Supporting Information) for the occupied levels near the HOMO, compared to the neutral one; i.e., the energy differences between the HOMO and other occupied MOs near the HOMO change little between the DNA in ionic and neutral states in water (see Table S19 in the Supporting Information).

This can be understood as follows. We note here that the first several occupied MOs near the HOMO of ODN GG in water are all localized on bases. The energy levels of MOs localized on a phosphate group are more than 1 eV lower than the energy level of HOMO in the water solvent, which is consistent with refs 29 and 30. Because the charge around the phosphate group is surrounded by the solvent water, its electrostatic effect on the MOs localized on bases is shielded. The magnitude of the energy shifts is consistent with the difference between the calculated IPs of a phosphorylated dinucleotide with and without Na^+ cations in solution.[30]

The geometries of the heavy atoms of ODN GG and ODN ^{Ph}GG (except the phenyl group) are not optimized in our calculations. (The geometries of the H atoms are optimized in both cases.) This is justified as follows. To see the effect of a geometry optimization, we compare IPs of a guanine with and without the geometry optimization by AM1 for heavy atoms. We are only interested in the energy shift that is due to the attachment of the phenyl group to the guanine; therefore, the difference of IPs between the guanine and phenylated guanine is important. The change of the geometry causes a change of the difference of IPs between the guanine and phenylated guanine where the geometry of the heavy atoms of a guanine is extracted from the fiber model structure, i.e., 0.05 and 0.04 eV for the 4th and 55th fiber model structures, respectively. The energy change due to the attachment of the phenyl group obtained by the Koopmans theorem is larger than those values.

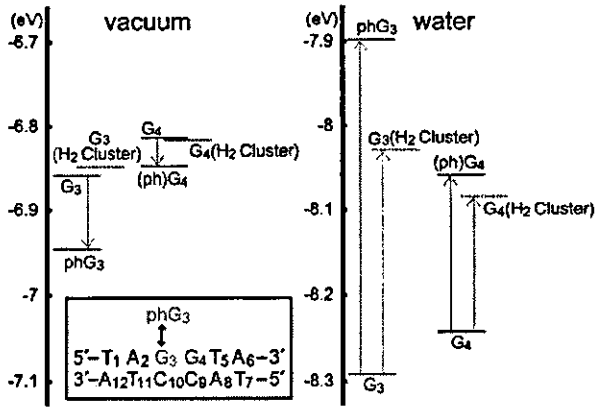

Figure 2. Energy shifts near the HOMO levels by the attachment of a phenyl group to G_3 with the 4th fiber model structure. Blue lines are for the energy levels of the G_3 localized orbitals, and red lines are for the energy levels of the G_4 localized orbitals. The energy levels of the DNA−H_2 cluster system, where the H_2 cluster mimics the solvent exclusion effect of the phenyl group (see Figure 4), are shown with dashed lines. The AM1/COSMO method is used. The energy level of MO localized on G_3 shifts to lower energy in a vacuum (left panel). In contrast, the same energy level shifts to higher energy in water (right panel). Inset shows the sequence of investigated double-stranded DNA.

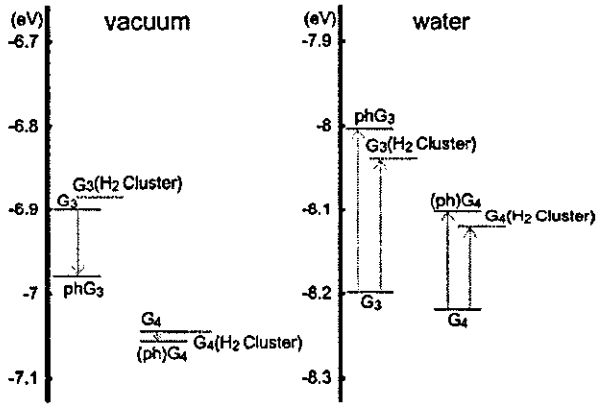

Figure 3. Energy shifts near the HOMO levels by the attachment of a phenyl group to G_3 with the 55th fiber model structure. Blue lines are for the energy levels of the G_3 localized orbitals, and red lines are for the energy levels of the G_4 localized orbitals. The energy levels of the DNA−H_2 cluster system, where the H_2 cluster mimics the solvent exclusion effect of the phenyl group (see Figure 4), are shown with dashed lines. The AM1/COSMO method is used. The energy level of MO localized on G_3 shifts to lower energy in a vacuum (left panel). In contrast, the same energy level shifts to higher energy in water (right panel). Inset shows the sequence of investigated double-stranded DNA.

3. Results and Discussion

3.1. Energy Shift of Molecular Orbital (MO) Localized on Guanine because of Phenyl Group Attachment and Comparison with Experiment. First, we show the results of the electronic structure calculation by AM1 with the COSMO model. The HOMO and HOMO-1 energy levels are shown in Figures 2 and 3. The bases that have the largest coefficients of the HOMO and HOMO-1 are indicated near the MO energy levels. (The MOs are highly localized on a base except ODN GG in water. The Coulomb interaction is strongly shielded in water; thus, the sequence dependence of the potential on each base due to the Coulomb interaction is rather suppressed. Therefore, the energy levels of G_3 and G_4 in water are almost degenerate and its HOMO and HOMO-1 levels are delocalized

TABLE 2: Energy Levels (in eV) of G_3 and G_4 Localized Orbitals of ODN GG and ODN ^{Ph}GG for the 4th and 55th Fiber Model Structures[a]

	vacuum		water	
	ODN GG	ODN ^{Ph}GG	ODN GG	ODN ^{Ph}GG
	4th fiber model			
G_3	−6.58	−6.64 (−0.05)	−8.11	−7.68 (0.43)
G_4	−6.75	−6.76 (−0.01)	−8.13	−7.91 (0.22)
	55th fiber model			
G_3	−6.67	−6.71 (−0.04)	−8.05	−7.80 (0.25)
G_4	−6.84	−6.89 (−0.05)	−8.08	−7.97 (0.11)

[a] The number in parentheses shows the energy shift (in eV) compared to the energy levels of ODN GG. The PM3/COSMO method is used.

TABLE 3: Energy Levels (in eV) of G_3 and G_4 Localized Orbitals of ODN GG and ODN ^{Ph}GG for the 4th Fiber Model Structure[a]

	vacuum		water	
	ODN GG	ODN ^{Ph}GG	ODN GG	ODN ^{Ph}GG
G_3	−3.925	−3.967 (−0.042)	−5.115	−5.039 (0.076)
G_4	−3.817	−3.850 (−0.033)	−5.002	−4.992 (0.010)

[a] The number in parentheses shows the energy shift (in eV) compared to the energy levels of ODN GG. The GB model implemented in the ab initio MO calculation program ABINIT/GB with the STO-3G basis set is used.

over those two bases.) Figures 2 and 3 indicate that attachment of a phenyl group to G_3 causes the following energy shifts of the HOMO and HOMO-1: (i) in a vacuum, the energy level of the G_3 localized orbital shifts to lower energy and the energy level of the G_4 localized orbital changes little, whereas (ii) in water, the energy levels of the localized orbitals of both G_3 and G_4 shift to higher values. The magnitude of change is larger for G_3. Consequently, the HOMO is localized on the phenylated guanine.

In addition, we have examined the solvent effect by different models, i.e., (i) the PM3 Hamiltonian[47] with the COSMO model in MOPAC2002 and (ii) the GB model[48] implemented in the ab initio MO/GB program package ABINIT/GB.[49] The ABINIT/GB program has been successfully applied to many systems (see, for example, ref 51). The PM3 calculation is conducted in a manner similar to that of the AM1 calculation explained in Section 2, except that the geometries of the H atoms and the phenyl group are optimized by the PM3 Hamiltonian. The energy shifts calculated by PM3 (Table 2) are very similar to those calculated by AM1 (see Figures 2 and 3). The ABINIT/GB calculations are performed with the STO-3G basis set. We use the 4th fiber model structure, and the geometries of the H atoms and the phenyl group are optimized by AM1. The energy shifts in Table 3 are again similar to those obtained by the AM1 calculations. These different types of calculations further confirm that the energy level of MO localized on G_3 shifts to higher value in water because of the attachment of a phenyl group to a guanine.

Experimentally, it has been observed that the introduction of N^2-phenyldeoxyguanosine significantly suppresses the oxidative decomposition at the phenylated base as well as other guanine bases.[14] Because the electronic energy levels of the phenylated guanine are higher than those of other guanine bases, the phenylated guanine has a greater chance to trap a hole than other guanine bases, which leads to the suppression of the oxidative decomposition of the guanine bases other than the phenylated one. The trapped hole experiences the annihilation processes

TABLE 4: Charge Distributions of HOMO, Which is Localized on the PhG_3[a]

	vacuum		water	
	G_3	phenyl group	G_3	phenyl group
4th fiber model	0.91	0.06	0.75	0.25
55th fiber model	0.94	0.05	0.89	0.10

[a] The AM1/COSMO method is used.

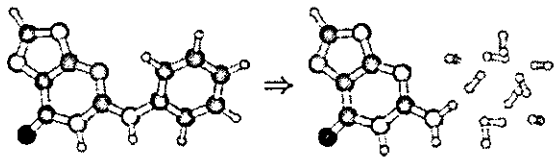

Figure 4. Structure of the H_2 cluster.

afterward, which results in the suppression of oxidative decomposition of the phenylated guanine.[14]

3.2. Origin of Energy Shift due to the Phenyl Group and Cases of Benzyl Group and *tert*-Butyl Group. The energy shifts shown in Section 3.1 are mainly due to the following two reasons: (i) the very existence of phenyl group prevents water molecules from approaching DNA, especially near the phenylated base; and (ii) attachment of a phenyl group to the guanine causes charge transfer between the phenyl group and guanine (see Table 4). To better understand them, we have conducted AM1/COSMO calculations of DNA with a H_2 cluster (10 H_2 molecules) in place of the phenyl group, where the H_2 cluster mimics the solvent-accessible surface of the phenyl group (see Figure 4). The geometry of the H_2 cluster is determined only from the geometry of the phenyl group, i.e., two H_2 molecules are assigned for each C−H of the phenyl group where one of four H atoms is placed at the position of the H atom of C−H and other three H atoms are placed around the C atom of C−H (see Tables S6, S9, S15, and S18 in the Supporting Information). Because there is little mixing between the MOs of G_3 and those of the H_2 cluster, we can selectively observe the effect of the exclusion of the solvent. The energy levels with the H_2 cluster are indicated by dashed lines in Figures 2 and 3. In a vacuum, the energy levels of the HOMO and HOMO-1 of the ODN GG-H_2 cluster system are very similar to those of ODN GG. This is expected because the existence of the H_2 cluster should have little effect on the energy levels of DNA. In water, on the other hand, the energy shift due to the H_2 cluster is similar to the shift due to the phenyl group, especially for the G_4 localized orbital. Because there is little charge transfer from G_4 to the phenyl group, the energy shifts of the G_4 localized orbital due to the phenyl group and the H_2 cluster are of the same origin, i.e., the solvent exclusion effect. In the case of the G_3 localized orbital, there is an additional effect on the energy shift due to charge transfer between the phenyl group and guanine (see Table 4). This may be the reason for the discrepancies between the energy shifts by the phenyl group and the H_2 cluster.

To further confirm the solvent exclusion effect, we have performed AM1/COSMO calculations of a DNA molecule with a benzyl group ($-CH_2C_6H_5$) attached instead of one with a phenyl group attached (i.e., a CH_2 spacer is inserted between the guanine and the phenyl group). We then compare the results to the corresponding DNA−H_2 cluster calculations (see Table 5). There is little charge transfer between the guanine and the phenyl group, because of the spacer. Therefore, we can expect that the MO energy levels near the HOMO without the benzyl group are similar to those with the H_2 cluster in a vacuum,

TABLE 5: Energy Levels (in eV) of G_3 and G_4 Localized Orbitals of ODN GG and a Benzyl-Group-Attached ODN GG, Which is Denoted as ODN ^{Bz}GG, for the 4th and 55th Fiber Model Structures[a]

	vacuum			water		
	ODN GG	ODN ^{Bz}GG	ODN GG + H_2 cluster	ODN GG	ODN ^{Bz}GG	ODN GG + H_2 cluster
			4th fiber model			
G_3	−6.86	−6.91 (−0.05)	−6.86 (0.00)	−8.29	−8.01 (0.28)	−8.03 (0.26)
G_4	−6.81	−6.96 (−0.15)	−6.82 (−0.01)	−8.24	−8.15 (0.09)	−8.10 (0.14)
			55th fiber model			
G_3	−6.90	−6.98 (−0.08)	−6.89 (0.01)	−8.20	−8.00 (0.20)	−8.03 (0.17)
G_4	−7.04	−7.16 (−0.12)	−7.05 (−0.01)	−8.22	−8.16 (0.06)	−8.13 (0.09)

[a] The energy levels (eV) of the ODN GG−H_2 cluster system, where the H_2 cluster mimics the solvent exclusion effect of the benzyl group, are also shown. The number in parentheses shows the energy shift (in eV) compared to the energy levels of ODN GG. The AM1/COSMO method is used.

TABLE 6: Energy Levels (in eV) of G_3 and G_4 Localized Orbitals of ODN GG and a *tert*-Butyl-Group-Attached ODN GG, Which is Denoted as ODN $^{t\text{-}Bu}$GG, for the 4th and 55th Fiber Model Structures[a]

	vacuum		water	
	ODN GG	ODN $^{t\text{-}Bu}$GG	ODN GG	ODN $^{t\text{-}Bu}$GG
		4th fiber model		
G_3	−6.86	−6.75 (0.11)	−8.29	−7.92 (0.37)
G_4	−6.81	−6.83 (−0.02)	−8.24	−8.08 (0.16)
		55th fiber model		
G_3	−6.90	−6.83 (0.07)	−8.20	−7.94 (0.26)
G_4	−7.04	−7.00 (0.04)	−8.22	−8.07 (0.15)

[a] The number in parentheses shows the energy shift (in eV) compared to the energy levels of ODN GG. The AM1/COSMO method is used.

whereas those with the benzyl group are similar to those with the H_2 cluster in water, because of the solvent exclusion effect. The results show that this is indeed the case. In water, the energy differences between the two HOMOs with the benzyl group and with the H_2 cluster are <0.02 eV (see Table 5). Please note that rather large energy shifts are found for G_4, because of the geometry of the benzyl group. For the 4th fiber model, the closest distance between the H atom in G_4 and the H atom in the benzyl group is 2.02 Å after the geometry optimization for the benzyl group by AM1.

If the large part of the energy shift is due to the solvent exclusion effect, a similar energy shift is expected by attaching an alkyl group to a guanine in a double-stranded ODN. Therefore, we have performed AM1/COSMO calculations of DNA with a *tert*-butyl group attached (i.e., the phenyl group is replaced by the *tert*-butyl group). As is expected, the energy shifts in water (Table 6) are similar to those with phenylated guanine (see Figures 2 and 3). On the other hand, unlike the phenylated case, the energy level of the G_3 localized orbital in a vacuum shifts to higher energy by ~0.1 eV. However, our assertion about the energy shift due to the solvent exclusion effect is still valid, because the energy shifts are larger in water than in a vacuum, by 0.27 and 0.19 eV in the 4th and 55th fiber model structures, respectively.

The reason for the energy shift to higher energy because of the solvent exclusion effect can be explained as follows. The MO levels near the HOMO of B-DNA shift to the lower energy in water compared to that in a vacuum. This is consistent with the finding that the energy levels of occupied MOs near the HOMO of a phosphorylated dinucleotide in a vacuum shift to lower energy in water.[30] (Note the difference of the energy levels for vacuum and for water in Figures 2 and 3.) When the phenyl group is attached to a base, the nearby bases experience a weaker solvent effect. As a result, the localized orbitals around the phenylated base shift to higher energies.

4. Conclusions

In conclusion, the energy level of a molecular orbital (MO) localized on a guanine shifts to lower value in a vacuum but to higher value in water, when a phenyl group is attached to the guanine base in a double-stranded DNA. This is mainly because the energy reduction of MO levels by the water solvent becomes smaller when the solvent is excluded by the phenyl group. As a result, we can expect that a phenylated guanine base has a greater chance to trap a hole in water. The observed suppression of the oxidative decomposition of guanines around the phenylated guanine[14] is thus explained in terms of the solvent effects. In addition, we have determined that the energy shifts due to the benzyl group or the *tert*-butyl group are similar to those that are due to the phenyl group in our calculation.

Supporting Information Available: Parameters used in the COSMO calculations; geometry used in the calculations (Tables S1−S18); comparison of the energy levels between DNA in neutral and ionic states in solution (Table S19). (PDF.) This material is available free of charge via the Internet at http://pubs.acs.org.

Acknowledgment. We are grateful to Dr. A. Klamt for the suggestions for the van der Waals parameters of COSMO. We are also thankful to Dr. T. Watanabe for his help related to the ABINIT/GB package. This research is supported by "Research and Development for Applying Advanced Computational Science and Technology" of Japan Science and Technology Corporation (ACT-JST).

Appendix: Evaluation of the Reorganization Energies

Let us denote the reorganization energy of a guanine base as λ_i^G and the solvent reorganization energy around the guanine as λ_s^G when a hole is injected to the guanine. The total reorganization energy around the guanine base λ^G then is given by

$$\lambda^G = \lambda_s^G + \lambda_i^G \tag{A1}$$

Similarly, we have

$$\lambda^{phG} = \lambda_s^{phG} + \lambda_i^{phG} \simeq \lambda_s^{phG} + \lambda_i^G + \lambda_i^{ph} \tag{A2}$$

Here, we assume that the reorganization energy of the phenylated guanine λ_i^{phG} can be approximated by the sum of λ_i^G and the reorganization energy of phenyl group λ_i^{ph}. Therefore, the difference of the reorganization energy between guanine and phenylated guanine is given by

$$\lambda^G - \lambda^{phG} \simeq \lambda_s^G - (\lambda_s^{phG} + \lambda_i^{ph}) \tag{A3}$$

The solvent reorganization energy of a DNA with a donor (guanine), an acceptor (diol), and a bridge has been reported as $\lambda_s = 0.27$ eV.[46] Because the diol is exposed to the solvent, the solvent reorganization energy around the donor is larger than that around the acceptor. Therefore, the reorganization energy due to the solvent around the guanine (λ_s^G) is expected to be less than a half of λ_s. When the phenyl group is attached to the guanine, the solvent reorganization energy λ_s^{phG} is smaller than λ_s^G. The energy reduction is partially compensated by the reorganization energy of the phenyl group (λ_i^{ph}). As a result, the change of the reorganization energy that is due to the attachment of the phenyl group to the guanine (eq A3) is expected to be <0.13 eV.

References and Notes

(1) Dekker, C.; Ratner, M. A. *Phys. World* **2001**, *14*, 29.

(2) (a) Grinstaff, M. W. *Angew. Chem., Int. Ed.* **1999**, *38*, 3629. (b) Schuster, G. B. *Acc. Chem. Res.* **2000**, *33*, 253. (c) Giese, B. *Acc. Chem. Res.* **2000**, *33*, 631.

(3) Lewis, F. D.; Letsinger, R. L.; Wasielewski, M. R. *Acc. Chem. Res.* **2001**, *34*, 159.

(4) (a) Porath, D.; Bezryadin, A.; de Vries, S.; Dekker, C. *Nature* **2000**, *403*, 635. (b) Yoo, K.-H.; Ha, D. H.; Lee, J.-O.; Park, J. W.; Kim, J.; Kim, J. J.; Lee, H.-Y.; Kawai, T.; Choi, H. Y. *Phys. Rev. Lett.* **2001**, *87*, 198102. (c) Watanabe, H.; Manabe, C.; Shigematsu, T.; Shimotani, K.; Shimizu, M. *Appl. Phys. Lett.* **2001**, *79*, 2462.

(5) (a) Fukui, K.; Tanaka, K. *Angew. Chem., Int. Ed.* **1998**, *37*, 158. (b) Kawai, K.; Takada, T.; Tojo, S.; Ichinose, N.; Majima, T. *J. Am. Chem. Soc.* **2001**, *123*, 12688. (c) Fukuzumi, S.; Nishimine, M.; Ohkubo, K.; Tkachenko, N. V.; Lemmetyinen, H. *J. Phys. Chem. B* **2003**, *107*, 12511.

(6) (a) Gasper, S. M.; Schuster, G. B. *J. Am. Chem. Soc.* **1997**, *119*, 12762. (b) Hall, D. B.; Holmlin, R. E.; Barton, J. K. *Nature* **1996**, *382*, 731. (c) Núñez, M. E.; Hall, D. B.; Barton, J. K. *Chem. Biol.* **1999**, *6*, 85. (d) Nakatani, K.; Dohno, C.; Saito, I. *J. Am. Chem. Soc.* **1999**, *121*, 10854.

(7) (a) Saito, I.; Takayama, M.; Sugiyama, H.; Nakatani, K. *J. Am. Chem. Soc.* **1995**, *117*, 6406. (b) Sugiyama, H.; Saito, I. *J. Am. Chem. Soc.* **1996**, *118*, 7063.

(8) Yoshioka, Y.; Kitagawa, Y.; Takano, Y.; Yamaguchi, K.; Nakamura, T.; Saito, I. *J. Am. Chem. Soc.* **1999**, *121*, 8712.

(9) (a) Tanielian, C.; Kobayashi, M.; Wolff, C. *J. Biomed. Opt.* **2001**, *6*, 252. (b) Kobayashi, M.; Koyama, S.; Nakazato, M.; Miyoshi, N.; Wolff, C.; Daikuzono, N.; Tanielian, C.; Sasaki, M.; Komiyama, M. *J. Clin. Laser Med. Surg.* **1994**, *12*, 133.

(10) (a) Ito, K.; Inoue, S.; Yamamoto, K.; Kawanishi, S. *J. Biol. Chem.* **1993**, *268*, 13221. (b) Oikawa, S.; Tada-Oikawa, S.; Kawanishi, S. *Biochemistry* **2001**, *40*, 4763.

(11) Voityuk, A. A.; Jortner, J.; Bixon, M.; Rösch, N. *Chem. Phys. Lett.* **2000**, *324*, 430.

(12) Zhu, Q.; LeBreton, P. R. *J. Am. Chem. Soc.* **2000**, *122*, 12824.

(13) Prat, F.; Houk, K. N.; Foote, C. S. *J. Am. Chem. Soc.* **1998**, *120*, 845.

(14) Nakatani, K.; Dohno, C.; Saito, I. *J. Am. Chem. Soc.* **2002**, *124*, 6802.

(15) (a) Bixon, M.; Giese, B.; Wessely, S.; Langenbacher, T.; Michel-Beyerle M. E.; Jortner, J. *Proc. Natl. Acad. Sci. U.S.A.* **1999**, *96*, 11713. (b) Voityuk, A. A.; Rösch, N.; Bixon, M.; Jortner, J. *J. Phys. Chem. B* **2000**, *104*, 9740.

(16) (a) Berlin, Y. A.; Burin, A. L.; Ratner, M. A. *J. Am. Chem. Soc.* **2001**, *123*, 260. (b) Grozema, F. C.; Siebbeles, L. D. A.; Berlin, Y. A.; Ratner, M. A. *Chem. Phys. Chem.* **2002**, *3*, 536.

(17) Okada, A.; Chernyak, V.; Mukamel, S. *J. Phys. Chem. A* **1998**, *102*, 1241.

(18) Okada, A.; Yokojima, S.; Kurita, N.; Sengoku, Y.; Tanaka, S. *J. Mol. Struct. (THEOCHEM)* **2003**, *630*, 283.

(19) (a) Priyadarshy, S.; Risser, S. M.; Beratan, D. N. *J. Phys. Chem.* **1996**, *100*, 17678. (b) Tong, G. S. M.; Kurnikov, I. V.; Beratan, D. N. *J. Phys. Chem. B* **2002**, *106*, 2381.

(20) Felts, A. K.; Pollard, W. T.; Friesner, R. A. *J. Phys. Chem.* **1995**, *99*, 2929.

(21) Segal, D.; Nitzan, A. *Chem. Phys.* **2002**, *281*, 235.

(22) (a) Li, X.-Q.; Yan, Y. J. *Appl. Phys. Lett.* **2001**, *79*, 2190. (b) Yan, Y. J.; Zhang, H. *J. Theor. Comput. Chem.* **2002**, *1*, 225.

(23) Conwell, E. M.; Rakhmanova, S. V. *Proc. Natl. Acad. Sci. U.S.A.* **2000**, *97*, 4556.

(24) Asai, Y. *J. Phys. Chem. B* **2003**, *107*, 4647.

(25) Kurnikov, I. V.; Tong, G. S. M.; Madrid, M.; Beratan, D. N. *J. Phys. Chem. B* **2002**, *106*, 7.

(26) Tanaka, S.; Sengoku, Y. *Phys. Rev. E* **2003**, *68*, 031905.

(27) Renger, T.; Marcus, R. A. *J. Phys. Chem. A* **2003**, *107*, 8404.

(28) Yoshioka, Y.; Kawai, H.; Sato, T.; Yamaguchi, K.; Saito, I. *J. Am. Chem. Soc.* **2003**, *125*, 1968.

(29) Kim, N. S.; LeBreton, P. R. *J. Am. Chem. Soc.* **1996**, *118*, 3694.

(30) Kim, N. S.; Zhu, Q.; LeBreton, P. R. *J. Am. Chem. Soc.* **1999**, *121*, 11516.

(31) Starikov, E. B. *Phys. Chem. Chem. Phys.* **2002**, *4*, 4523.

(32) Gervasio, F. L.; Carloni, P.; Parrinello, M. *Phys. Rev. Lett.* **2002**, *89*, 108102.

(33) Reynisson, J.; Schuster, G. B.; Howerton, S. B.; Williams, L. D.; Barnett, R. N.; Cleveland, C. L.; Landman, U.; Harrit, N.; Chaires, J. B. *J. Am. Chem. Soc.* **2003**, *125*, 2072.

(34) Kino, K.; Saito, I.; Sugiyama, H. *J. Am. Chem. Soc.* **1998**, *120*, 7373.

(35) Cadet, J.; Berger, M.; Buchko, G. W.; Joshi, P. C.; Raoul, S.; Ravanat, J.-L. *J. Am. Chem. Soc.* **1994**, *116*, 7403.

(36) Vialas, C.; Pratviel, G.; Claparols, C.; Meunier, B. *J. Am. Chem. Soc.* **1998**, *120*, 11548.

(37) Lu, X.-J.; Shakked, Z.; Olson, W. K. *J. Mol. Biol.* **2000**, *300*, 819.

(38) (a) Arnott, S. Polynucleotide Secondary Structures: An Historical Perspective. In *Oxford Handbook of Nucleic Acid Structure*; Neidle, S., Ed.: Oxford University Press: New York, 1999; pp 1−38. (b) Chandrasekaran, R.; Arnott, S. *J. Biomol. Struct. Dyn.* **1996**, *13*, 1015.

(39) Premilat S.; Albiser, G. *Nucleic Acids Res.* **1983**, *11*, 1897.

(40) (a) Dewar, M. J. S.; Zoebisch, E. G.; Healy, E. F.; Stewart, J. J. P. *J. Am. Chem. Soc.* **1985**, *107*, 3902. (b) Dewar, M. J. S.; Jie, C. *J. Mol. Struct. (THEOCHEM)* **1989**, *187*, 1.

(41) Stewart, J. J. P., Fujitsu Limited, Tokyo, Japan, 2001.

(42) Klamt, A.; Schüürmann, G. *J. Chem. Soc., Perkin Trans.* **1993**, *2*, 799.

(43) Klamt, A.; Jonas, V.; Bürger, T.; Lohrenz, J. C. W. *J. Phys. Chem. A* **1998**, *102*, 5074.

(44) Hush, N. S.; Cheung, A. S. *Chem. Phys. Lett.* **1975**, *34*, 11.

(45) Seidel, C. A. M.; Schulz, A.; Sauer, M. H. M. *J. Phys. Chem.* **1996**, *100*, 5541.

(46) Lewis, F. D.; Kalgutkar, R. S.; Wu, Y.; Liu, X.; Liu, J.; Hayes, R. T.; Miller, S. E.; Wasielewski, M. R. *J. Am. Chem. Soc.* **2000**, *122*, 12346.

(47) Stewart, J. J. P. *J. Comput. Chem.* **1989**, *10*, 209.

(48) (a) Born, M. Z. *Phys.* **1920**, *1*, 45. (b) Hoijtink, G. J.; de Boer, E.; van der Meij, P. H.; Weijland, W. P. *Recl. Trav. Chim. Pay−Bas.* **1956**, *75*, 487. (c) Jano, I. *C. R. Acad. Sci.* **1965**, *261*, 103.

(49) Kikuchi, O.; Morihashi, K.; Takahashi, O.; Nakano, T.; Ogawa, Y.; Inadomi, Y. ABINIT/GB, Ab Initio MO/GB Program Package; University of Tsukuba: Tsukuba, Japan, 1999.

(50) Klamt, A., personal communication.

(51) (a) Kikuchi, O.; Watanabe, T.; Ogawa, Y.; Takase, H.; Takahashi, O. *J. Phys. Org. Chem.* **1997**, *10*, 145. (b) Watanabe, T.; Hashimoto, K.; Takase, H.; Kikuchi, O. *J. Mol. Struct. (THEOCHEM)* **1997**, *397*, 113.

Available online at www.sciencedirect.com
SCIENCE DIRECT®
Bioorganic & Medicinal Chemistry
ELSEVIER
Bioorganic & Medicinal Chemistry 12 (2004) 3117–3123

The binding of guanine–guanine mismatched DNA to naphthyridine dimer immobilized sensor surfaces: kinetic aspects

Kazuhiko Nakatani,[a,b,*] Akio Kobori,[b] Hiroyuki Kumasawa,[a] Yuki Goto[a] and Isao Saito[a]

[a]*Department of Synthetic Chemistry and Biological Chemistry, Faculty of Engineering, Kyoto University, Kyoto 615-8510, Japan*
[b]*PRESTO, Japan Science and Technology Agency (JST), Kyoto 615-8510, Japan*

Received 15 March 2004; revised 8 April 2004; accepted 8 April 2004
Available online 10 May 2004

Abstract—Naphthyridine dimer composed of two naphthyridine chromophores and a linker connecting them strongly, and selectively, binds to the guanine–guanine mismatch in duplex DNA. The kinetics for the binding of the G–G mismatch to the naphthyridine dimer was investigated by surface plasmon resonance assay. The sensor surface was prepared by immobilizing naphthyridine dimer through a long poly(ethylene oxide) linker with the ligand density of 9.1×10^{-12} fmol nm^{-2}. The kinetic analyses revealed that the binding of the G–G mismatch was sequence dependent on the flanking base pairs, and the G–G mismatches flanking at least one G–C base pair bound to the surface via a two-step process with a 1:1 DNA–ligand stoichiometry. The first association rate constant for the binding of the G–G mismatch in the 5′-CGG-3′/3′-GGC-5′ sequence to the naphthyridine dimer-immobilized sensor surface was 3.2×10^{3} M^{-1} s^{-1} and the first dissociation rate constant was 1.4×10^{-2} s^{-1}. The association and dissociation rate constants for the second step were insensitive to the flanking sequences, and were almost of the same order of magnitude as the first dissociation rate constant. This indicates that the second step had only a small energetic contribution to the binding. The association constant calculated from kinetic parameters was 2.7×10^{5} M^{-1}, which is significantly smaller than the apparent association constants obtained from experiments in solution. Electrospray ionization time-of-flight (ESI-TOF) mass spectrometry on the complex produced from the G–G mismatch and naphthyridine dimer showed the formation of the 1:1 complex and a 1:2 DNA–ligand complex in solution. The latter complex became the dominant complex when a six-fold excess of naphthyridine dimer was added to DNA.

1. Introduction

Heteroduplex analyses[1,2] are the methods that used for the typing of single nucleotide polymorphisms (SNPs) in testing sample DNAs by detecting the mismatched base pairs in heteroduplex produced by strand exchange between sample and the standard DNAs.[3–5] The absence of the mismatched base pairs in a heteroduplex indicated the absence of SNPs in the testing DNAs. Conventional methods for the detection of mismatched base pairs in heteroduplex analyses were enzymatic and chemical cleavage at the mismatched sites,[6–8] gel electrophoresis,[2,9] and selective capture by mismatch-binding proteins.[10,11] We,[12–18] and others,[19–21] have pursued a modified method of heteroduplex analyses for the SNPs detection by using small molecular ligands that can selectively bind to the mismatched base pairs. Molecules binding to the mismatched base pairs in heteroduplex can substitute these low-throughput methods. We have developed novel sensors for a surface plasmon resonance (SPR) assay to detect the G–G,[12] G–A,[17] and C–C[18] mismatch duplexes. The G–G mismatch-detecting sensor was prepared by immobilizing naphthyridine dimer **1**,[12] which strongly and selectively binds to the G–G mismatch.[13] SPR detects the change in the refractive index caused by variation of the mass on the sensor chip surface for example, when the analyte binds to the immobilized ligand on the surface. The change in SPR signal, termed the SPR response presented in resonance units (RU), is directly related to the change in surface concentration of biomolecules. SPR response of 1000 RU is equivalent to the change in surface concentration of 1 ng/mm^2. Thus, the density of immobilized ligands on the surface and amount of analyte bound to the surface could be calculated by the difference in SPR response before and after the analyses. The SPR signal is monitored continuously so that chemical interaction between ligand and DNA can be studied in real time.[22] Naphthyridine dimer **1** (Chart 1) consisted of two 2-amino-7-methyl-1,8-naphthyridines having complementary

Keywords: Mismatch; Kinetics; SPR; Naphthyridine.
* Corresponding author. Tel.: +81-75-383-2756; fax: +81-75-383-2759; e-mail: nakatani@sbchem.kyoto-u.ac.jp

0968-0896/$ - see front matter © 2004 Elsevier Ltd. All rights reserved.
doi:10.1016/j.bmc.2004.04.005

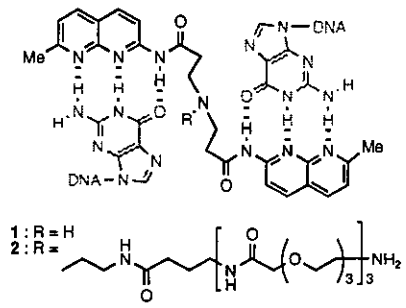

Chart 1. Structures of naphthyridine dimers and their hydrogen bonding to guanines.

surface of hydrogen bonding to a guanine and a linker connecting two chromophores. The sensor surface could differentiate DNA containing the G–G mismatch from that containing normal and other mismatched base pairs.

In addition to the thermodynamic studies, kinetic analysis on the binding of the G–G mismatch to the sensor would provide important information for the molecular design of ligands targeting other mismatched base pairs, and for improving the sensor sensitivity. The density of the ligand immobilized on the surface of SPR sensors significantly affects the sensitivity and the binding kinetics.[23,24] Sensors having a high ligand density on the surface are suitable for the detection of the analyte at low concentrations, whereas those having a low number of ligands on the surface are recommended for kinetic analysis. With the sensor surfaces that had a high ligand density, most of the analyte in the solution was bound to the surface, which increased the sensitivity of the sensor. However, under these conditions, the degree of binding was probably controlled by the rate of mass transport of the analyte from the bulk solution to the surface. This phenomenon, known as mass transport limitation, yields incorrect kinetic parameters for ligand–analyte binding.[25–28] It is also conceivable that, for the sensor surface with a high ligand density, the binding of the analyte to the surface may involve more than one ligand, which would result in complex binding kinetics. In this paper, we have examined the kinetics of the binding of the G–G mismatch duplex to the surface with regard to a different sequence flanking to the mismatch. The kinetic analyses revealed that (1) the binding of the G–G mismatch was found sequence dependent on the flanking base pairs, (2) the G–G mismatches flanking at least one G–C base pair bind to the surface via a two-step process with a 1:1 DNA–ligand stoichiometry, (3) the first association rate constant largely determines the over all efficiency of the binding, and (4) at an excess of ligand concentration a complex with a 1:2 DNA–ligand ratio became predominant.

2. Results and discussion

2.1. Preparation of naphthyridine dimer immobilized sensor surfaces

Naphthyridine dimer **2** tethered to a long poly(ethylene oxide) (PEO) linker was immobilized on an activated

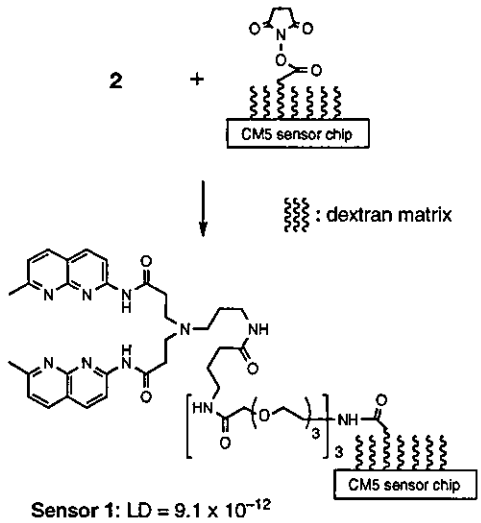

Scheme 1. Synthesis of naphthyridine dimer immobilized sensors. (LD, fmol nm^{-2}).

carboxyl terminal attached to the dextran surface according to the procedure recommended by Biacore (Scheme 1).[29] Immobilization of **1** to the SPR sensor through a long PEO linker was found to significantly increase the SPR intensity.[30] Thus, a 1 mM solution of **2** having a primary amino group at the linker termini in 10 mM of a borate buffer (pH = 9.2) was applied to the carboxylic acid of the CM5 sensor chip activated with *N*-hydroxysuccinimide and EDCI. The degree of immobilization of the ligands was monitored by the increasing SPR signal, and controlled by changing the reaction time. After immobilization of the ligand, the activated esters that remained intact on the surface were destroyed by treating them with ethanolamine. We synthesized a **2**-immobilized sensor surface (**Sensor 1**) by immobilizing **2** for 10 response units (RU). **Sensor 1** had a ligand density on the sensor surface of 9.1×10^{-12} fmol nm^{-2} (1 RU = 1 pg mm^{-2}). Thus, one molecule of **2** existed in an area of ca. 14×14 nm^2 on the surface. Under such an extremely low ligand density, it is reasonable to assume that only one naphthyridine dimer was involved in the binding of the G–G mismatch to the surface.

2.2. Determination of the binding model

Before the kinetic analysis, the binding model of the interaction between the G–G mismatch and **1** was investigated by fitting the sensorgrams to a theoretical binding curve. The 27-mer duplex 5′-d(GTT ACA GAA TCT **XGY** AAG CCT AAT ACG)-3′/3′-d(CAA TGT CTT AGA **X′GY′** TTC GGA TTA TGC)-5′ containing the G–G mismatch (**XGY/X′GY′** = **CGG/GGC**) was applied to **Sensor 1** at DNA concentrations of 2, 5, and 10 μM. All the SPR measurements were carried out at a temperature of 5 °C. The observed sensorgrams were analyzed by a simultaneous curve fitting method for all the sensorgrams and also by an individual curve fitting of each sensorgram using Marquardt–Levenberg

algorithms (Fig. 1).[31] With both methods, it was confirmed that the sensorgrams fit well to a two-state binding model (Eq. 1). However, neither fitted well to simple bimolecular, heterogeneous, nor bivalent binding models. According to the curve fitting by two-state binding model, the SPR response could be resolved into two components, that is, SPR response due to the first state forming **(CGG/GGC–1)$_A$** from G–G with **1** and the following step producing **(CGG/GGC–1)$_B$** from **(CGG/GGC–1)$_A$** (Fig. 2). Because of two-state binding, the fraction of **(CGG/GGC–1)$_A$** and **(CGG/GGC–1)$_B$** in the total complex bound to the surface was dependent on the association time. After 90 s of association, the fraction of **(CGG/GGC–1)$_A$** and **(CGG/GGC–1)$_B$** were 11.5 and 5.1 RU, whereas it became 12.2 and 9.9 RU after 180 s.

$$\text{CGG/GGC} + \mathbf{1} \underset{k_{d1}}{\overset{k_{a1}}{\rightleftharpoons}} \mathbf{(CGG/GGC\text{–}1)_A} \underset{k_{d2}}{\overset{k_{a2}}{\rightleftharpoons}} \mathbf{(CGG/GGC\text{–}1)_B} \quad (1)$$

To confirm the two-state binding model, the binding of **CGG/GGC** to **Sensor 1** was examined for different

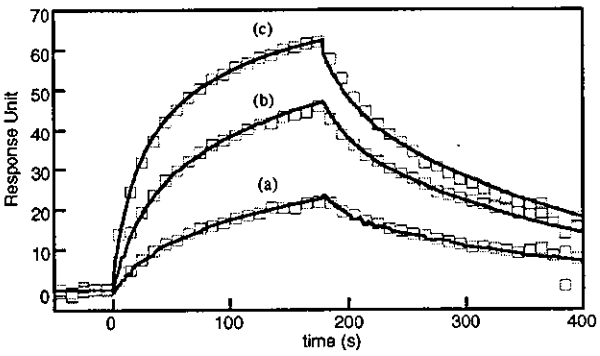

Figure 1. Binding of **CGG/GGC** to **Sensor 1** at different DNA concentrations. Binding was measured for 180 s and dissociation for 220 s. DNA concentration was (a) 2, (b) 5, and (c) 10 μM. Experimental curves (open square) were overlaid with the fitted curves (solid lines) to the two-state model.

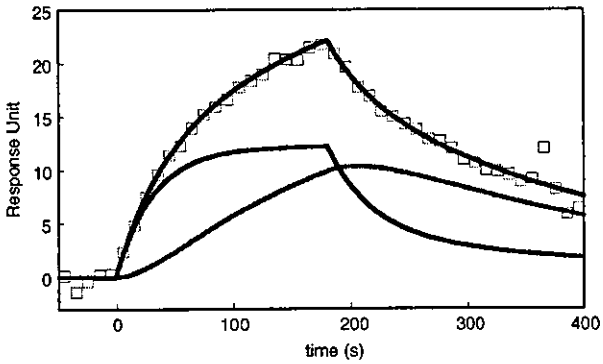

Figure 2. Sensorgram of 2 μM **CGG/GGC** to **Sensor 1**. Shown is the experimental curve (red square) overlaid with the fitted curve (solid black line) from two-state binding model. Simulated curves displaying the initial binding (solid blue line) and subsequence binding (solid green line) are the additive components from the fitted curve.

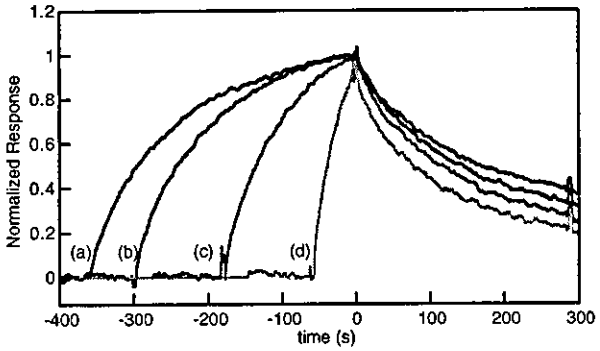

Figure 3. Binding of **CGG/GGC** (2 μM) at different association periods to **Sensor 1**. Association period was (a) 360, (b) 300, (c) 180, and (d) 60 s. Dissociation was measured for 300 s. Response curves were overlaid by zeroing the start of the dissociation phase. Observed responses were normalized by setting the response at the start of the dissociation phase (time = 0 s) to 1.0.

association periods.[24] In the case of simple bimolecular binding, the dissociation curves obtained for different association periods would be superimposable by normalizing the SPR intensity. In contrast, the dissociation curves would not superimpose when the binding involved two states, because the ratio of the two complexes (e.g., **(CGG/GGC–1)$_A$** and **(CGG/GGC–1)$_B$**) at the initial state of the dissociation phase would be time-dependent on the association phase. As can be seen from Figure 3, the dissociation curves obtained for the association periods of 60, 180, 300, and 360 s showed different dissociation profiles, and were not superimposable on each other. A rapid dissociation was observed with 60 s of association, whereas a much slower dissociation was observed when the G–G mismatch duplex was contacted to the sensor for 360 s. When a bivalent binding (i.e., two molecules of naphthyridine dimer on the surface sequentially bind to the G–G mismatch site) was involved in the interaction between **Sensor 1** and **CGG/GGC**, the dissociation curves were not superimposable. However, bivalent binding was excluded in this particular case, because of the extremely low density of immobilized **2** on **Sensor 1**. On the basis of these experimental results, the binding of the G–G mismatch to **Sensor 1** was concluded to proceed via two states, with the DNA–ligand ratio for the binding being 1:1. While SPR detects the change of the molecular mass on the sensor surface, it has been reported that kinetic analysis can determines the conformational change of the analyte bound on the surface.[32,33] The binding of the G–G mismatch to **Sensor 1** described here is considered as the case.

2.3. Effect of the flanking sequence on the binding kinetics

The kinetics for the binding of the G–G mismatch DNA to **Sensor 1** were investigated regarding the 10 flanking sequences **(XGY/X′GY′)** (Fig. 4). The sensorgrams obtained for the **CGC/GGG**, **TGG/AGC**, **GGC/CGG**, **TGC/AGG**, **AGG/TGC**, **AGC/TGG**, and **AGA/TGT** resembled those of **CGG/GGC** in shape, which validates

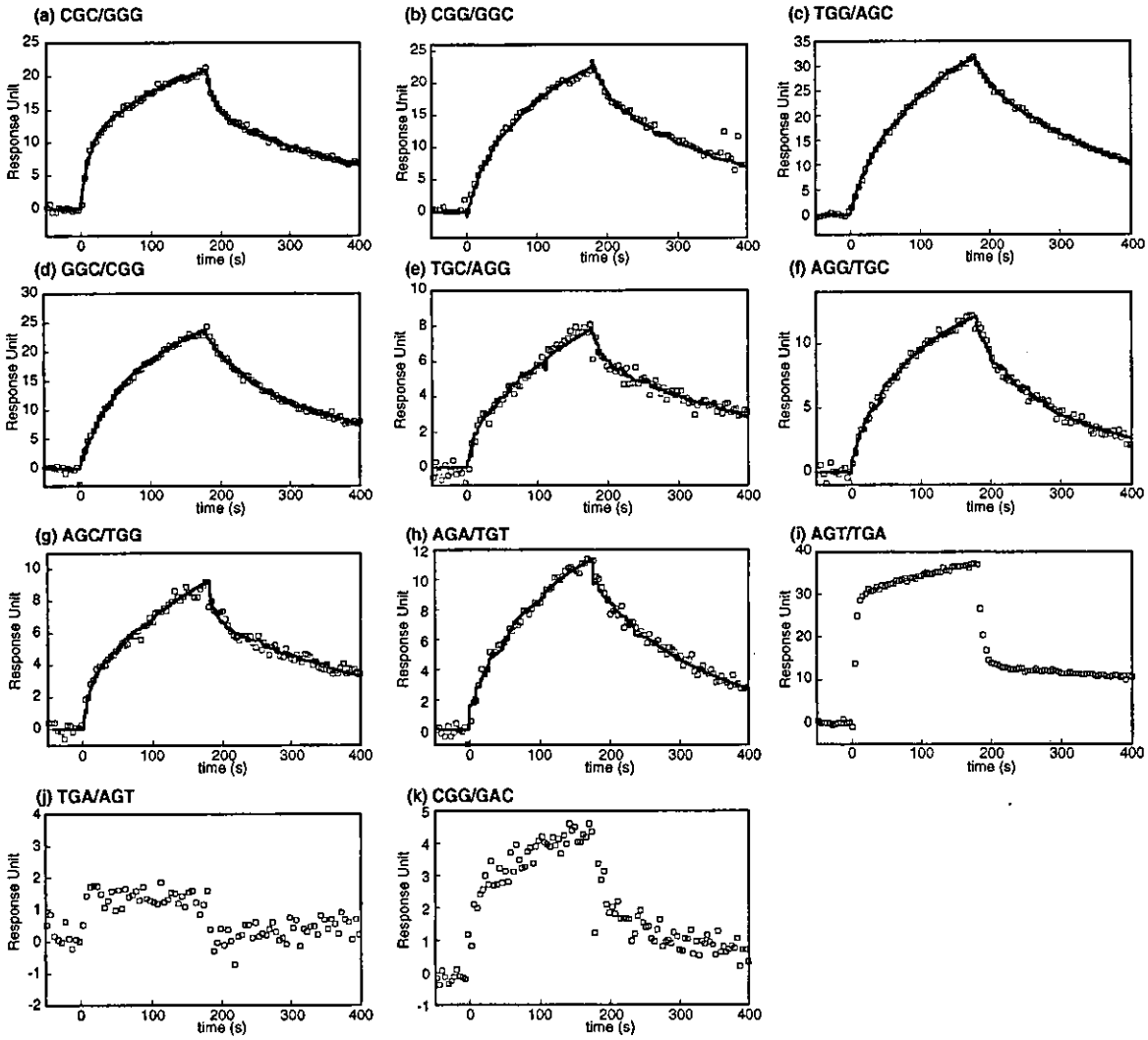

Figure 4. Sensorgrams obtained for the binding of **XGY/X′GY′** to **Sensor 1** at the concentration of 2 μM duplex. Binding was measured for 180 s and dissociation for 220 s. Experimental data (open square) were overlaid with the fitted curve (solid line) to the two-state model except (i), (j), and (k). Key: (a) **CGC/GGG**, (b) **CGG/GGC**, (c) **TGG/AGC**, (d) **GGC/CGG**, (e) **TGC/AGG**, (f) **AGG/TGC**, (g) **AGC/TGG**, (h) **AGA/TGT**, (i) **AGT/TGA**, (j) **TGA/AGT**, (k) **CGG/GAC**.

the analysis of these sensorgrams using a two-state model. In contrast, the sensorgrams obtained for the **AGT/TGA** and **TGA/AGT**, which have A–T base pairs flanking the mismatch, showed a rapid increase and decrease in SPR intensity, and were considerably different in shape from the other sensorgrams. Therefore, analysis using a two-state model was not feasible for these two sequences. It is worth noting that the G–G mismatch in **AGA/TGT**, where one guanine was flanked by two adenines, showed sensorgrams resembling that of **CGG/GGC**, which could be analyzed by using the two-state model.

The kinetic parameters for the eight G–G mismatches were obtained by fitting the sensorgrams at a duplex concentration of 2 μM to the theoretical curve of the two-state model supplied by BIAcore (Table 1). The four kinetic parameters obtained for **CGG/GGC** were $3.2\times10^{3}\,M^{-1}\,s^{-1}$ for the first association rate constant (k_{a1}), $1.4\times10^{-2}\,s^{-1}$ for the first dissociation rate constant (k_{d1}), $0.8\times10^{-2}\,s^{-1}$ for the second association rate constant (k_{a2}), and $6.6\times10^{-3}\,s^{-1}$ for the second dissociation rate constant (k_{d2}). The magnitude of the first association rate constant, k_{a1}, was sequence dependent. The value of k_{d1} was around $10^{-2}\,s^{-1}$, and it did not show any obvious sequence dependence. The rate constants k_{a2} and k_{d2} for the second step were insensitive to the flanking sequences, and were almost of the same order of magnitude as k_{d1}. The equilibrium constant for the second binding step is in the range of 0.4–4 for all G–G mismatches, suggesting that the second step does not directly correlated to the recognition of the G–G mismatches by **1**. The reorganization of the bound DNA duplex on the sensor surfaces is most plausible. These kinetic data suggest that the important binding events involving the intercalation of the naphthyridine chro-

Table 1. Association and dissociation rate constants for the binding of the G–G mismatch duplexes to **Sensor 1**[a]

5′-XYZ-3′ 3′-X′Y′Z′-5′	K_a (M^{-1})	K_{a1} ($M^{-1}s^{-1}$)	K_{d1} (s^{-1})	K_{a2} (s^{-1})	K_{d2} (s^{-1})
CGC **GGG**	5.0×10^5	9.4×10^3	5.6×10^{-2}	1.3×10^{-2}	4.4×10^{-3}
CGG **GGC**	2.7×10^5	3.2×10^3	1.4×10^{-2}	0.8×10^{-2}	6.6×10^{-3}
TGG **AGC**	2.5×10^5	2.8×10^3	3.5×10^{-2}	2.8×10^{-2}	8.8×10^{-3}
GGC **CGG**	1.9×10^5	2.5×10^3	1.4×10^{-2}	6.6×10^{-3}	6.1×10^{-3}
TGC **AGG**	1.3×10^5	1.7×10^3	6.0×10^{-2}	2.0×10^{-2}	4.5×10^{-3}
AGG **TGC**	5.1×10^4	1.1×10^3	1.4×10^{-2}	4.9×10^{-3}	7.6×10^{-3}
AGC **TGG**	3.6×10^4	3.9×10^2	4.5×10^{-2}	1.8×10^{-2}	4.5×10^{-3}
AGA **TGT**	3.5×10^4	8.4×10^2	8.7×10^{-3}	4.3×10^{-3}	1.2×10^{-2}
ACT **TGA**	ND[b]	ND	ND	ND	ND
TGA **ACT**	ND	ND	ND	ND	ND
CGG **GAC**	ND	ND	ND	ND	ND

[a] The K_a values were derived from the equation: $K_a = k_{a1}k_{a2}/k_{d1}k_{d2}$.
[b] Not determined due to the inconsistency of the binding model.

mophore onto the mismatched site, the formation of the hydrogen bonds between naphthyridine and the guanine, and a conformational change of the duplex occur in the first step. The magnitude of k_{a1} ranged from $3.9\times10^2\,M^{-1}s^{-1}$ for **AGC/TGG**, to $9.4\times10^3\,M^{-1}s^{-1}$ for **CGC/GGG**. The value of k_{a1} increased with increasing number of G–C base pairs in the flanking sequence. The G–G mismatches flanking the A–T base pairs were less thermodynamically stable than were those flanking the G–C base pairs.[34] This is rationalized by the improved stacking stabilization of the G–G mismatch by the flanking G–C base pairs compared with the A–T base pairs.[35,36] The observed sequence dependence of k_{a1} may suggest that a partial stacking stabilization of the incoming naphthyridine chromophore into the mismatched site by the flanking G–C base pair(s) accelerates the binding. The G–G mismatches in the **AGT/TGA** and **TGA/AGT** having no G–C base pairs in the flanking sequence would be flexible in structure due to weak stacking stabilization of the mismatched base pair, and susceptible to intercalative binding with the naphthyridine chromophore. The complexes thus formed, however, are not stabilized by stacking with the flanking A–T base pairs, and this results in a rapid dissociation of the complex. The binding of the G–G mismatches flanking the G–C base pairs to the naphthyridine dimer is much slower than that of the G–G mismatches flanking the A–T base pairs. This is most likely due to the greater energy required for the conformational change of the stacked mismatched base pair.

The binding of the G–A mismatch to **Sensor 1** was studied to elucidate the kinetics of the binding of **1** to the G–G mismatch from binding to a nonconsensus mismatch. The SPR signals obtained for the G–A mismatch having two G–C base pairs in the flanking sequence (**CGG/GAC**) were weak, and the shape of the sensorgrams was in-between those of the extremes of **CGG/GGC** and **AGA/TGT**. Therefore, analysis of the sensorgrams using the two-state model was not feasible with **Sensor 1**. While the G–A mismatch in **CGG/GAC** was flanked by two G–C base pairs, the sensorgrams showed a rather rapid association and dissociation. Because the thermodynamic stability of **CGG/GAC** judged from its melting temperature is comparable to that of **CGG/GGC**,[12] the rapid association and dissociation may be attributable to an inconsistency in the surface of the hydrogen bonding between the G–A mismatch site and the naphthyridine dimers.

2.4. Implication for the binding model in solution

The association constant of $K_a = 2.7\times10^5\,M^{-1}$ for **CGG/GGC** calculated from the four kinetic parameters ($K_a = (k_{a1}\cdot k_{a2})/(k_{d1}\cdot k_{d2})$) is significantly smaller than the apparent K_a of $1.9\times10^7\,M^{-1}$ and $9.1\times10^6\,M^{-1}$ obtained in our earlier experiments using DNase I footprint titration and isothermal titration calorimetry (ITC), respectively.[12,14,37] The inconsistency of the results we obtained in these studies using **Sensor 1** with

those obtained in solution is most likely due to a low ligand density of **Sensor 1**, and suggests that a different binding model may be involved in the solution phase. This hypothesis was supported by the observations that the binding of **CGG/GGC** to a **1**-immobilized sensor with an increased ligand density by 50-fold to 4.7×10^{-10} fmol nm^{-2} (cf. 9.1×10^{-12} fmol nm^{-2} for **Sensor 1**) became stronger for all G–G mismatches, but no more fit to 1:1 binding model (data not shown). To gain insight into the binding in solution phase, the complex of the 11-mer duplex 5′-d(CTA ACG GAA TG)-3′/3′-d(GAT TGG CTT AC)-5′ (**cgg/ggc**) containing the G–G mismatch in the sequence of 5′CGG3′/3′GGC5′ and **1** was analyzed by electrospray ionization time of flight mass spectrometry (ESI-TOF MS).[38] When **cgg/ggc** (20 μM) and **1** (20 μM) were mixed in a 1:1 ratio in 100 mM of ammonium acetate in 50% methanol solution, we observed the $[M-5H]^{5-}$ ions corresponding to the 1:1 (**cgg/ggc–1**) and the 1:2 (**cgg/ggc–1·1**) complexes as well as the $[M-5H]^{5-}$ ions of the intact duplex (Fig. 5). The 1:2 DNA–ligand complex became dominant in the mass spectra in the presence of a sixfold excess of **1** in solution. These results suggested that, in addition to the 1:1 binding, a 1:2 binding could also contribute to the high affinity of **1** to the G–G mismatch in solution under a high DNA–ligand ratio (Eq. 2). While the structure of the 1:2 complex discovered in these studies is beyond our knowledge at this moment, the sequence dependence of the SPR intensity obtained by **Sensor 1** may implicate the binding of naphthyridine dimer not only to the G–G mismatch but also to the flanking base pairs.

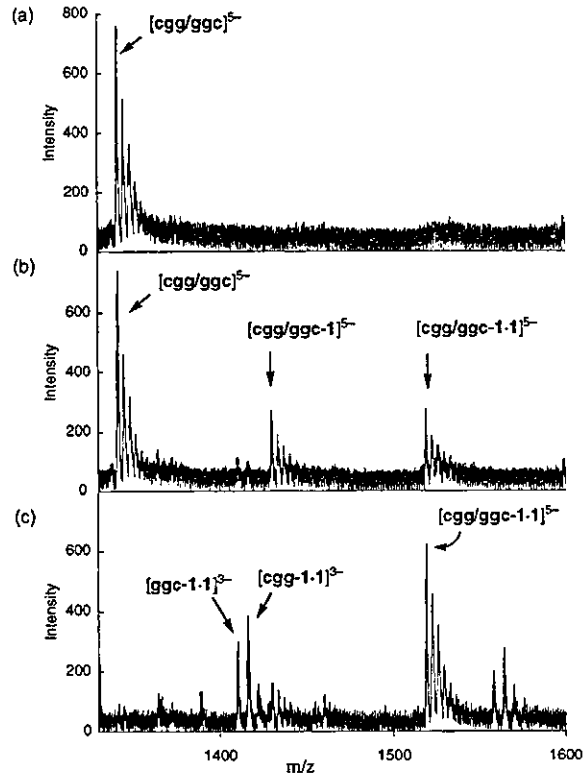

Figure 5. ESI-TOF mass spectra of 11-mer duplex **cgg/ggc** in the absence and presence of **1**. Samples contained 20 μM duplex in 50% aqueous methanol and 100 mM NH_4OAc with **1** at a concentration of (a) 0, (b) 20, and (c) 120 μM. For clarity, the range of m/z from 1330 to 1600 was shown. The ions of the indicated composition accompanied by ions of ammonium adducts.

$$\textbf{cgg/ggc} + \textbf{1} \rightleftharpoons \textbf{cgg/ggc-1} \overset{\textbf{1}}{\rightleftharpoons} \textbf{cgg/ggc-1·1} \quad (2)$$

3. Conclusions

The kinetic analysis of the G–G mismatch to **Sensor 1** confirmed the 1:1 binding. The binding involves two steps, and the efficiency of the binding is governed by the rate of the first binding step of the mismatch to the naphthyridine dimer. In addition to the 1:1 binding, ESI-MS measurements on the complex showed that a bivalent binding mode was also involved in the binding in solution. These observations are important clues for the design of novel ligands that strongly and selectively bind to the mismatched sites.

4. Experimental

4.1. Immobilization of naphthyridine dimer to the surface of SPR sensors

All immobilization were performed in HBS-N running buffer (0.01 M HEPES, pH 7.4, 0.15 M NaCl) using Biacore2000 instrument (Biacore, Uppsala, Sweden) at 25 °C. Naphthyridine dimer **2** was attached to the dextran surface of the sensor chip (CM5, Biacore) following a 10 min activation of surface carboxyl groups using a 1:1 mixture of 1-(3-dimethylaminopropyl)-3-ethylcarbodiimide hydrochloride (EDCI) (1 M) and *N*-hydroxysuccinimide (0.25 M) with a flow rate of 5 μL/min. A 1 mM solution of **2** in 10 mM borate buffer (pH 9.2) was injected until the desired level of response units (RU) had been reached. One flow channel was always left as a blank for a reference. Following attachment, the remaining carboxyl groups on the surface were quenched with 35 μL of 1 M ethanolamine, pH 8.5 with a flow rate of 10 μL/min.

4.2. SPR measurements

SPR measurements were performed in HBS-N running buffer at 4 or 25 °C. Binding was measured for 180 s and dissociation for 220 s before regeneration unless otherwise noted. DNA samples bound on the surface were removed following each measurement by using 7 M urea as regeneration solution at 100 μL/min for 24 min.

4.3. Kinetic analysis of sensorgrams

Response curves used for the fitting were prepared by subtracting the signal generated simultaneously on the flow cell for the control. The response curves obtained for various concentrations of analyte were globally or locally fitted to binding models supplied with the ana-

lytical software of BIA evaluation 3.0. These include simple bimolecular (A + B to AB), heterogeneous (A + B to AB1; A + B2 to AB2), the two-state (A + B to AB then to ABx), and a bivalent analyte (A + B to AB and AB + B to ABB) binding models.

4.4. ESI-TOF measurements

ESI-TOF measurements were carried out with JEOL AccuTOF equipment. A solution containing 11-mer duplex containing a mismatch (20 μM) and **1** (20 μM) in 100 mM of ammonium acetate in 50% methanol solution was injected into the ionization chamber.

Acknowledgements

This work was supported by Grant-in-Aid for Scientific Research on Priority Areas (C) 'Medical Genome Science' from the Ministry of Education, Culture, Sports, Science and Technology of Japan.

References and notes

1. Landers, J. P. *Anal. Chem.* **2003**, *75*, 2919–2927.
2. Nataraj, A. J.; Olivos-Glander, I.; Kusukawa, N. *Electrophoresis* **1999**, *20*, 1177–1185.
3. Syvänen, A.-C. *Nat. Rev. Genet.* **2001**, *2*, 930–942.
4. Kwok, P. Y. *Annu. Rev. Genom. Hum. G.* **2001**, *2*, 235–258.
5. Schafer, A. J.; Hawkins, J. R. *Nat. Biotechnol.* **1998**, *16*, 33–39.
6. Myers, R. M.; Larin, Z.; Maniatis, T. *Science* **1985**, *230*, 1242–1246.
7. Rowley, G.; Saad, S.; Giannelli, F.; Green, P. M. *Genomics* **1995**, *30*, 574–582.
8. Roberts, E.; Deeble, V. J.; Woods, C. G.; Taylor, G. R. *Nucliec Acids Res.* **1997**, *25*, 3377–3378.
9. White, M. B.; Carvalho, M.; Derse, D.; O'Brien, S. J.; Dean, M. *Genomics* **1992**, *12*, 301–306.
10. Fazakerley, G. V.; Qignard, E.; Woisard, A.; Guschlbauer, W.; van der Marel, G. A.; van Boom, J. H.; Jones, M.; Radman, M. *EMBO J.* **1986**, *5*, 3697–3703.
11. Smith, J.; Modrich, P. *Proc. Natl. Acad. Sci. U.S.A.* **1996**, *93*, 4374–4379.
12. Nakatani, K.; Sando, S.; Saito, I. *Nat. Biotechnol.* **2001**, *19*, 51–55.
13. Nakatani, K.; Sando, S.; Kumasawa, H.; Kikuchi, J.; Saito, I. *J. Am. Chem. Soc.* **2001**, *123*, 12650–12657.
14. Nakatani, K.; Sando, S.; Saito, I. *Bioorg. Med. Chem.* **2001**, *9*, 2381–2385.
15. Smith, E. A.; Kyo, M.; Kumasawa, H.; Nakatani, K.; Saito, I.; Corn, R. M. *J. Am. Chem. Soc.* **2002**, *124*, 6810–6811.
16. Nakatani, K.; Hagihara, S.; Sando, S.; Sakamoto, S.; Yamaguchi, K.; Maesawa, C.; Saito, I. *J. Am. Chem. Soc.* **2003**, *125*, 662–666.
17. Hagihara, S.; Kumasawa, H.; Goto, Y.; Hayashi, G.; Kobori, A.; Saito, I.; Nakatani, K. *Nucliec Acids Res.* **2004**, *32*, 278–286.
18. Kobori, A.; Horie, S.; Suda, H.; Saito, I.; Nakatani, K. *J. Am. Chem. Soc.* **2004**, *126*, 557–562.
19. Jackson, B. A.; Barton, J. K. *J. Am. Chem. Soc.* **1997**, *119*, 12986–12987.
20. Jackson, B. A.; Alekseyev, V. Y.; Barton, J. K. *Biochemistry* **1999**, *38*, 4655–4662.
21. Lacy, E. R.; Cox, K. K.; Wilson, W. D.; Lee, M. *Nucleic Acids Res.* **2002**, *30*, 1834–1841.
22. Pharmacia-Biosensor. 1990 *Biacore User's Manual.* Piscatway, NJ.
23. Myszka, D. G. *Curr. Opin. Biotechnol.* **1997**, *8*, 50–57.
24. Myszka, D. G.; Wood, S. J.; Biere, A. L. *Methods Enzymol.* **1999**, *309*, 386–402.
25. Glaser, R. W. *Anal. Biochem.* **1993**, *213*, 152–161.
26. Nygren, H.; Werthen, M.; Stenberg, M. *J. Immunol. Methods* **1987**, *101*, 63–71.
27. Stenberg, M.; Nygren, H. *J. Theor. Biol.* **1985**, *113*, 129–140.
28. Bertozzi, C. R.; Bednarski, M. D. *J. Org. Chem.* **1991**, *56*, 4326–4329.
29. Löfås, S.; Johnson, B. *J. Chem. Soc., Chem. Commun.* **1990**, *21*, 1526–1528.
30. Nakatani, K.; Kobori, A.; Kumasawa, H.; Saito, I. *Bioorg. Med. Chem. Lett.* **2004**, *14*, 1105–1108.
31. Morton, T. A.; Myszka, D. G.; Chaiken, I. M. *Anal. Biochem.* **1995**, *227*, 176–185.
32. Sota, H.; Hasegawa, Y.; Iwakura, M. *Anal. Chem.* **1998**, *70*, 2019–2024.
33. Jenkins, J. L.; Lee, M. K.; Valaitis, A. P.; Curtiss, A. C.; Dean, D. H. *J. Biol. Chem.* **2000**, *275*, 14423–14431.
34. Peyret, N.; Seneviratne, P. A.; Allwi, H. T.; SntaLucia, J., Jr. *Biochemistry* **1999**, *38*, 3468–3477.
35. Sponer, J.; Leszczynski, J.; Hobza, P. *J. Phys. Chem.* **1996**, *100*, 5591–5596.
36. Alhambra, C.; Luque, F. J.; Gago, F.; Orozco, M. *J. Phys. Chem.* **1997**, *101*, 3846–3853.
37. It is worth noting that the association constants obtained by DNase I footprint titration assumed a 1:1 binding stoichiometry. Therefore, these were referred as apparent K_a.
38. Beck, J. L.; Colgrave, M. L.; Ralph, S. F.; Sheil, M. M. *Mass Spectrom. Rev.* **2001**, *20*, 61–87.

Available online at www.sciencedirect.com
SCIENCE DIRECT®
Bioorganic & Medicinal Chemistry Letters
ELSEVIER
Bioorganic & Medicinal Chemistry Letters 14 (2004) 3431–3433

2-Ureidoquinoline: a useful molecular element for stabilizing single cytosine and thymine bulges

Akio Kobori,[b] Takashi Murase,[a] Hitoshi Suda,[a] Isao Saito[a] and Kazuhiko Nakatani[a,b,*]

[a]*Department of Synthetic Chemistry and Biological Chemistry, Faculty of Engineering, Kyoto University, Kyoto 615-8510, Japan*
[b]*PRESTO, Japan Science and Technology Agency (JST), Kyoto 615-8510, Japan*

Received 2 April 2004; revised 22 April 2004; accepted 23 April 2004

Abstract—We have demonstrated that aromatic heterocycles having hydrogen-bonding surfaces complementary to those of nucleotide bases are effective molecular elements for the binding to single nucleotide bulges and base mismatches. We here report that a new molecule, 2-ureidoquinoline having an alignment of hydrogen-bonding groups in the order of acceptor–donor–donor stabilizes single cytosine and thymine bulges in duplex DNAs. Furthermore, a dimeric form of 2-ureidoquinoline stabilizes cytosine–cytosine and cytosine–thymine mismatches.

Having completed a sequence analysis of human genome, effective detections of genetic mutations became an indispensable technology in many research fields of molecular biology, genetics, and chemical biology.[1–3] Binding of small molecular probes to single nucleotide bulges and base mismatches in duplex DNA provides an innovative method in heteroduplex analysis of deletion and insertion mutations as well as single nucleotide polymorphisms (SNPs).[4–6] We have demonstrated that aromatic heterocycles having hydrogen-bonding surfaces complementary to those of nucleotide bases are effective molecular elements for the binding to single nucleotide bulges and base mismatches.[7–15] *N*-Acyl-2-amino-1,8-naphthyridine in which the hydrogen-bonding groups are aligned in the order of acceptor–acceptor–donor stabilized a duplex containing a guanine bulge.[7] Guanine–guanine mismatches were strongly stabilized by a form of covalently linked dimer.[8] In addition to the strong preferences of *N*-acyl-2-amino-1,8-naphthyridine to a guanine base, a modest stabilization of the cytosine bulge was also observed. Since the hydrogen-bonding surface of the molecule was partially matched to that of a cytosine, these observations prompted us to modulate the hydrogen-bonding surface of the molecule to be fully complementary to a cytosine.

We here report that a new molecule, 2-ureidoquinoline having an alignment of hydrogen-bonding groups in the order of acceptor–donor–donor stabilizes single cytosine and thymine bulges in duplex DNAs. Furthermore, a dimeric form of 2-ureidoquinoline stabilizes cytosine–cytosine and cytosine–thymine mismatches (Figs. 1 and 2).

We have synthesized a series of molecules **1a–d** having different aromatic heterocycles with a side chain containing a urea structure. These molecules were obtained by a coupling of corresponding amino-substituted heterocycles with *N*-Boc-4-isocyanatobutylamine, that was prepared by the reaction of *N*-Boc-5-aminovaleric acid and diphenylphosphoryl azide. The effect of these compounds having urea structures on the stabilization

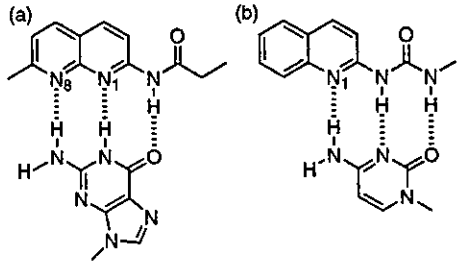

Figure 1. Possible hydrogen bonding between (a) *N*-acyl-2-amino-1,8-naphthyridine and guanine, and (b) 2-ureidoquinoline and cytosine.

Keywords: Ureidoquinoline; Bulge; Mismatch.
* Corresponding author. Tel.: +81-75-383-2756; fax: +81-75-383-2759; e-mail: nakatani@sbchem.kyoto-u.ac.jp

0960-894X/$ - see front matter © 2004 Elsevier Ltd. All rights reserved.
doi:10.1016/j.bmcl.2004.04.075

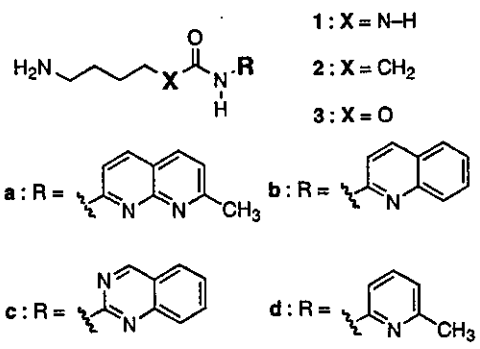

Figure 2. Molecules examined in these studies.

of a single nucleotide bulge in duplex DNA was compared with corresponding amide compounds **2a** and **2b** as well as quinolinylcarbamate **3b**. Amide compounds were synthesized by the coupling of amino heterocycles with pentafluorophenyl *N*-Boc-6-aminohexanoate, whereas **3b** was obtained by Curtius rearrangement of quinaldic acid followed by a coupling with *N*-Boc-aminobutanol. Deprotection of the Boc group furnished the synthesis of all molecules. The number of atoms between the carbonyl carbon to the terminal amino group in the linker was kept constant for all molecules. The effects of these molecules on a stabilization of a single nucleotide bulge were investigated by measuring a melting temperature (T_m) of duplexes 5′-d(TCC AG GCA AC)-3′/3′-d(AGG TCX CGT TG)-5′ containing a single nucleotide bulge at the position of **X**. The difference of the melting temperature (ΔT_m) in the absence and presence of the molecule (100 μM) in sodium cacodylate buffer (10 mM, pH 7.0) was summarized in Table 1.

In the presence of **1a** consisting of a naphthyridine ring and a urea linker, T_m was increased for all duplexes-containing single nucleotide bulges, but not for the fully matched 11-mer duplex. ΔT_m for cytosine, thymine, guanine, and adenine bulges were 4.8, 3.7, 2.4, and 3.1 °C, respectively. Ureidoquinoline **1b** that was lacked by one ring nitrogen compared to **1a** showed a comparable ΔT_m for cytosine and thymine bulges, but a decreased ΔT_m for guanine and adenine bulges. Ureidoquinazoline **1c**, where only one of two ring nitrogens can simultaneously participate in the hydrogen bonding to the bulged nucleotide, showed much lower ΔT_m for all bulges than **1b**. Truncation of naphthyridine and quinoline rings to a pyridine ring as in **1d** resulted in a complete loss of stabilizing effects of bulged duplexes. The significance of a urea structure of **1a** and **1b** for the stabilization of single nucleotide bulges was clearly demonstrated by comparing the ΔT_m values with those obtained by the corresponding amide compounds **2a** and **2b**. The ΔT_m obtained for the cytosine, thymine, and adenine bulges in the presence of **2a** was decreased by 3.8, 3.7, and 3.2 °C, respectively, from those obtained in the presence of **1a**, but the ΔT_m for the guanine bulge was slightly increased instead. A similar propensity of ΔT_m values was observed for **2b**. Quinolinylcarbamate **3b** where one hydrogen donor in a urea structure was replaced by hydrogen acceptor exhibited a median effect on the stabilization of single nucleotide bulges.

Comparing **1a** with **1b** and also **1b** with **2b**, the nitrogen at a position 8 of 1,8-naphthyridine was not necessary for the stabilization of cytosine, thymine, and adenine bulges, but hydrogen-bonding donor of a urea group was essential. The low ability of **1c** for the stabilization of single nucleotide bulges is most likely due to a conformational variety regarding the urea group. Conformational calculations of **1c** indicated that hydrogen bonding between N3 of quinazoline and N–H in urea would be stable by forming six-membered ring.[16] In that conformation, hydrogen-bonding groups aligned in the order of acceptor–donor–acceptor. Preorganization of hydrogen groups was reported an important factor for producing a stable hydrogen-bonded complex.[17–20] Marked modulations of the ΔT_m observed by changing N–H in **1b** into methylene and oxygen in **2b** and **3b**, respectively, clearly demonstrated the effect of hydrogen-bonding interactions on the stabilization of single nucleotide bulges.

Having found that ureidoquinoline **1b** effectively stabilized the cytosine and thymine bulges, the potential for the stabilization of a base mismatch by a dimeric form of **1b** was investigated. Ureidoquinoline dimer **4** was synthesized by a reductive amination of aldehyde **5** with primary amine **6**, which were obtained by a common precursor of phenylcarbamate (Scheme 1).[21] ΔT_m values for the base mismatches were obtained from the melting temperatures of 11-mer duplex containing a single base mismatch (X–Y) in the middle of the sequence (Table 2).

Table 1. Increased T_m (°C) of bulge-containing duplexes in the presence of testing molecules[a]

Drug	5′-d(TCCAG_GCAAC)-3′ 3′-d(AGGTCXCGTTG)-5′				Match (11-mer)
	X: C	T	G	A	
1a	4.8	3.7	2.4	3.1	−0.3
1b	4.9	4.2	1.8	2.6	−0.4
1c	1.1	1.4	−1.9	−0.1	−0.6
1d	0.8	0.0	−0.1	0.1	−0.7
2a	1.0	0.0	2.9	−0.1	0.2
2b	1.0	0.2	0.6	0.1	−0.1
3b	2.2	1.9	1.0	0.9	0.0

[a] [DNA base] = 100 μM, [ligand] = 100 μM, [NaCl] = 100 mM, [sodium cacodylate] = 10 mM (pH 7.0).

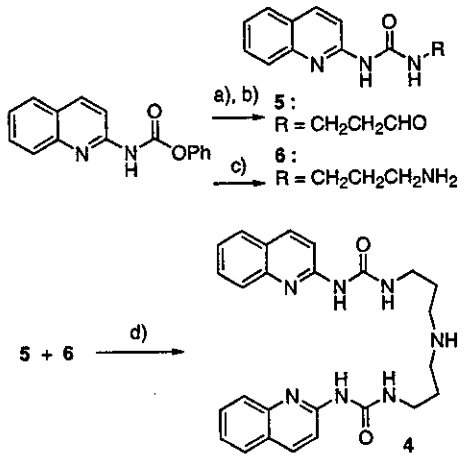

Scheme 1. Reagents and conditions: (a) 3,3-diethoxypropylamine, (b) AcOH, H_2O, 99% (two steps), (c) propylenediamine, 79%, (d) 5+6, $NaBH_3CN$, AcOH, MeOH, 54%.

Table 2. Increased T_m (°C) of mismatch-containing duplexes in the presence of 4[a]

5′-d(CTAACXGAATG)-3′ 3′-d(GATTGYCTTAC)-5′			
X–Y	ΔT_m	X–Y	ΔT_m
C–C	6.8	G–T	1.0
C–T	6.1	T–T	0.5
C–A	2.4	A–A	−0.2
G–G	2.4	G–C	0.0
G–A	2.0	A–T	−0.8

[a] [DNA base] = 100 μM, [ligand] = 100 μM, [NaCl] = 100 mM, [sodium cacodylate] = 10 mM (pH 7.0).

The ΔT_m of 6.8 °C was observed for the C–C mismatch, whereas the fully matched duplexes where X–Y were G–C and A–T were not stabilized at all under the same conditions. In marked contrast to dimer **4**, little increase of the T_m was observed for the C–C mismatch in the presence of ureidoquinoline **1b**, demonstrating that a covalent connection of two ureidoquinolines is quite effective for the stabilization of the C–C mismatch.[22] The ΔT_m of 6.1 °C was also observed for the C–T mismatch. Other mismatches including C–A, G–G, G–A, G–T, A–A, and T–T showed a small increase of their T_m values. Stabilization of C–C and C–T mismatches by **4** is consistent with that a monomeric form **1b** stabilize cytosine and thymine bulges. A complete failure of stabilizing the thymine–thymine mismatch by **4** implies that the stabilization of thymine–thymine mismatch needs a different strategy from that used for the G–G and C–C mismatches, although we have so far succeeded in stabilizing base mismatches by utilizing a dimeric form of bulge-stabilizing molecules.

In conclusion, ureidoquinolines were found a good molecular element for stabilizing single cytosine and thymine bulges. Integration of this binding element into its dimeric form provides a molecule stabilizing cytosine–cytosine and cytosine–thymine mismatches.

Acknowledgements

This work was supported by Grant-in-Aid for Scientific Research on Priority Areas (C) 'Medical Genome Science' from the Ministry of Education, Culture, Sports, Science and Technology of Japan.

References and notes

1. Syvänen, A.-C. *Nature Rev. Genet.* **2001**, *2*, 930–942.
2. Kwok, P. Y. *Annu. Rev. Genom. Hum. G.* **2001**, *2*, 235–258.
3. Schafer, A. J.; Hawkins, J. R. *Nat. Biotechnol.* **1998**, *16*, 33–39.
4. Jackson, B. A.; Barton, J. K. *J. Am. Chem. Soc.* **1997**, *119*, 12986–12987.
5. Jackson, B. A.; Alekseyev, V. Y.; Barton, J. K. *Biochemistry* **1999**, *38*, 4655–4662.
6. Lacy, E. R.; Cox, K. K.; Wilson, W. D.; Lee, M. *Nucleic Acids Res.* **2002**, *30*, 1834–1841.
7. Nakatani, K.; Sando, S.; Saito, I. *J. Am. Chem. Soc.* **2000**, *122*, 2172–2177.
8. Nakatani, K.; Sando, S.; Saito, I. *Nat. Biotechnol.* **2001**, *19*, 51–55.
9. Nakatani, K.; Sando, S.; Kumasawa, H.; Kikuchi, J.; Saito, I. *J. Am. Chem. Soc.* **2001**, *123*, 12650–12657.
10. Nakatani, K.; Sando, S.; Saito, I. *Bioorg. Med. Chem.* **2001**, *9*, 2381–2385.
11. Smith, E. A.; Kyo, M.; Kumasawa, H.; Nakatani, K.; Saito, I.; Corn, R. M. *J. Am. Chem. Soc.* **2002**, *124*, 6810–6811.
12. Nakatani, K.; Hagihara, S.; Sando, S.; Sakamoto, S.; Yamaguchi, K.; Maesawa, C.; Saito, I. *J. Am. Chem. Soc.* **2003**, *125*, 662–666.
13. Kobori, A.; Horie, S.; Suda, H.; Saito, I.; Nakatani, K. *J. Am. Chem. Soc.* **2004**, *126*, 557–562.
14. Hagihara, S.; Kumasawa, H.; Goto, Y.; Hayashi, G.; Kobori, A.; Saito, I.; Nakatani, K. *Nucleic Acids Res.* **2004**, *32*, 278–286.
15. Nakatani, K.; Kobori, A.; Kumasawa, H.; Saito, I. *Bioorg. Med. Chem. Lett.* **2004**, *14*, 1105–1108.
16. Although a similar cyclic conformation involving internal hydrogen bonding was also conceivable for **1b**, energy differences between cyclic and linear conformations were smaller for **1b** than **1c**.
17. Jorgensen, W. L.; Pranata, J. *J. Am. Chem. Soc.* **1990**, *112*, 2008–2010.
18. Pranata, J.; Wierschke, S. G.; Jorgensen, W. L. *J. Am. Chem. Soc.* **1991**, *113*, 2810–2819.
19. Sartorius, J.; Schneider, H. J. *Chem. Eur. J.* **1996**, *2*, 1446–1452.
20. Murray, T. J.; Zimmerman, S. C. *J. Am. Chem. Soc.* **1992**, *114*, 4010–4011.
21. Sigmund, H.; Pfleiderer, W. *Helv. Chim. Acta* **1994**, *77*, 1267–1280.
22. ΔT_m of 0.1 °C was observed for C–C mismatch in the presence of ureidoquinoline **1b** at the concentration of 100 μM in 100 mM sodium cacodylate buffer (pH 7.0) containing 100 mM NaCl.

Available online at www.sciencedirect.com
SCIENCE DIRECT®
Bioorganic & Medicinal Chemistry Letters
ELSEVIER
Bioorganic & Medicinal Chemistry Letters 15 (2005) 259–262

A new ligand binding to G–G mismatch having improved thermal and alkaline stability

Tao Peng,[b] Takashi Murase,[a] Yuki Goto,[a] Akio Kobori[b] and Kazuhiko Nakatani[a,b,*]

[a]*Department of Synthetic Chemistry and Biological Chemistry, Faculty of Engineering, Kyoto University, Kyoto 606-8501, Japan*
[b]*PRESTO, Japan Science and Technology Agency (JST), Kyoto 615-8510, Japan*

Received 4 October 2004; revised 28 October 2004; accepted 30 October 2004
Available online 21 November 2004

Abstract—Naphthyridine dimer (ND) specially binds to guanine–guanine (G–G) mismatch in duplex DNA. In order to improve the thermal and alkaline stability and binding ability of the ligand, we have examined structural modification of the linker. A new ligand (NNC) possessing 2-amino-1,8-naphthyridines and a carbamate linker is much more thermally stable than ND. The half-life of NNC is 2.5 times longer than that of ND at 80 °C. NNC is also much more stable than ND under alkaline conditions. In addition, NNC binds to G–G mismatch more strongly than ND. The improved stability and the binding of NNC to the G–G mismatch would be suitable for the practical use of NNC-immobilized sensor.

Since a draft sequence of the human genome was determined,[1,2] some 1.6 million human single nucleotide polymorphisms (SNPs) have been found in the human genome and deposited to public databases.[3] SNPs became extremely important as a genetic marker for the identification of disease genes and detection of genetic mutations.[4,5] Thus, simple and rapid detection of a single nucleotide difference in the DNA sequences is an indispensable technique for both SNP mapping and typing. Although a number of methods have been developed for SNPs typing,[4,6,7] there is still a great need for designing new typing methods that are simple in operation, rapid and accurate in analysis, and low in cost.

We have recently reported a novel approach for the detection of SNPs by sensing guanine–guanine (G–G) mismatches in duplex DNA.[8] We have developed a sensor chip that can detect G–G mismatches in duplex DNA by means of surface plasmon resonance (SPR).[9,10] The sensor was prepared by immobilizing mismatch binding ligand naphthyridine dimer (ND) onto the carboxylated dextran matrix on the gold surface. We have reported that ND binds selectively to G–G mismatches in duplex DNA.[8,11] During the regeneration process of the ND-immobilized surface under alkaline conditions after each mismatch analysis, it was observed that the immobilized ND was slowly degraded under the conditions. We also found that high temperature necessary for denaturing the bound duplex on ND-immobilized sensor induced the ND degradation. Improving the thermal and alkaline stability of the mismatch-binding ligand eventually leads to a prolonged sensor lifetime. We report here a novel G–G mismatch binding ligand (NNC) that has not only greatly improved thermal and alkaline stability but also the higher affinity and selectivity to the G–G mismatch compared to ND (Fig. 1).

To gain insights into the degradation pathway, we first examined the thermal reaction of ND at 80 °C in 100 mM sodium cacodylate (pH 7.0) by HPLC (Fig. 2).

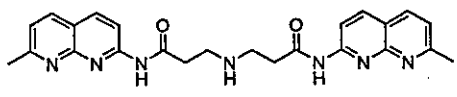

ND

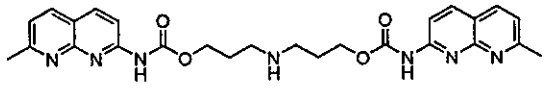

NNC

Figure 1. ND and NNC.

Keywords: DNA; Recognition; Mismatch.
* Corresponding author. Tel.: +81 753832756; fax: +81 753832759; e-mail: nakatani@sbchem.kyoto-u.ac.jp

0960-894X/$ - see front matter © 2004 Elsevier Ltd. All rights reserved.
doi:10.1016/j.bmcl.2004.11.003

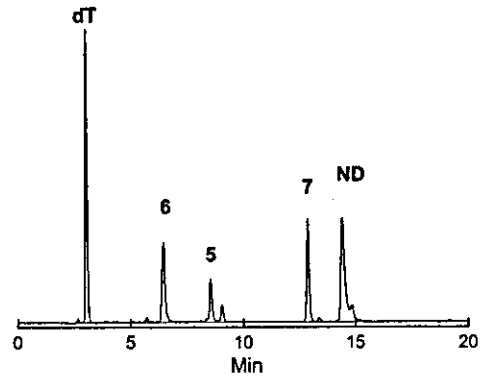

Figure 2. HPLC profile for the thermolysis of ND (0.71 mM) in 100 mM sodium cacodylate buffer (pH 7.0) for 45 min at 80 °C. dT was added as an internal standard.

The dT was selected as an internal standard for the thermolysis so that the reproducible and quantitative data could be obtained from the chromatographs. We detected three major products, which were identified as 2-amino-7-methyl-1,8-naphthyridine (**5**), 3-amino-*N*-(7-methyl-1,8-naphthyridin-2-yl)-propionamide (**6**), and *N*-(7-methyl-1,8-naphthyridin-2-yl)-acrylamide (**7**). The formation of **5** suggested the hydrolysis of the amide linkage, where as β-elimination was another degradation pathway producing **6** and **7** (Fig. 3).

To suppress both degradation processes and retain the binding ability to the G–G mismatch, a new molecule **NNC**, where amide linkage was substituted by a carbamate linkage, was synthesized. In addition, the alkyl chain length was further extended by one carbon for each side to slow down the nucleophilic addition of the secondary amino group in the linker to the carbonyl group leading to a release of **5**.

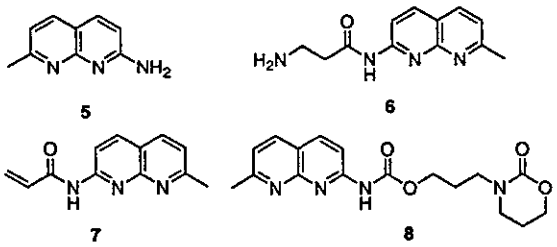

Figure 3. The products derived from thermolysis of ND and NNC.

NNC was synthesized as shown in Scheme 1. *N*-Boc-dipropanolamine was reacted with *N*,*N*′-disuccinimidyl carbonate (DSC) in dry acetonitrile to produce carbonate,[12] which was then reacted with 2-amino-7-methyl-1,8-naphthyridine to afford Boc-protected **NNC**. Deprotection by hydrogen chloride in ethyl acetate gave hydrochloride salt of **NNC**.[13]

The thermal reaction of **NNC** was examined under the same condition as that of **ND** (Fig. 4).

The major products of the **NNC** degradation after incubating at 80 °C for 120 min were identified as **5** and (7-methyl-1,8-naphthyridin-2-yl)-carbamic acid 3-(2-oxo-1,3-oxazinan-3-yl)-propyl ester (**8**) (Fig. 3). After a periodic incubation, the amount of **ND** and **NNC** were analyzed by HPLC. The rate of thermolysis could be determined from the decrease of the ligands. The half-life curves for the thermolysis of **NNC** and **ND** were shown in Figure 5. It is clearly shown that the half-life of **ND** is about 40 min at 80 °C, whereas the half-life of

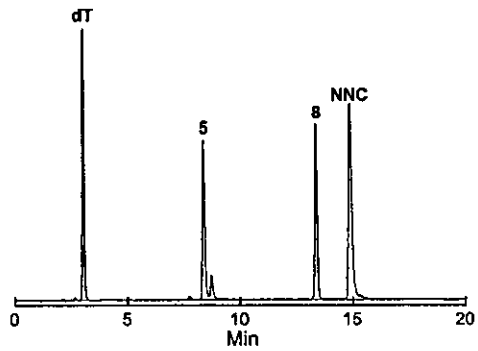

Figure 4. HPLC profile for the thermolysis of NNC (0.71 mM) in 100 mM sodium cacodylate buffer (pH 7.0) for 120 min at 80 °C.

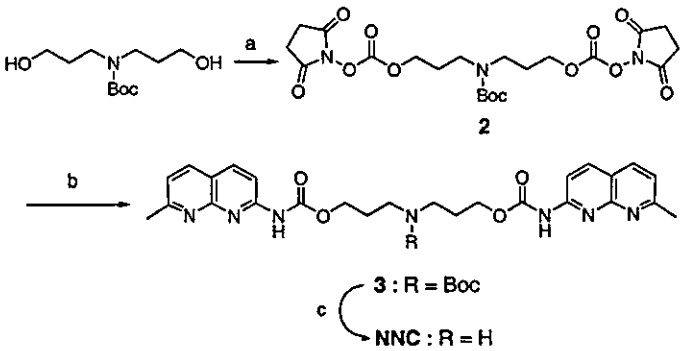

Scheme 1. Reagents and conditions: (a) *N*,*N*′-disuccinimidyl carbonate, CH_3CN, Et_3N; (b) 2-amino-7-methyl-1,8-naphthyridine, CH_2Cl_2, Et_3N, 49% for two steps; (c) HCl, AcOEt, $CHCl_3$, quantitative.